Characterizing sources of high surface ozone events in the southwestern U.S. with intensive field measurements and two global models

Li Zhang[1,2*], Meiyun Lin[1,2*], Andrew O. Langford[3], Larry W. Horowitz[2], Christoph J. Senff[3,4], Elizabeth Klovenski[5], Yuxuan Wang[5], Raul J. Alvarez II[3], Irina Petropavlovskikh[3,4], Patrick Cullis[3,4], Chance W. Sterling[3,4,6], Jeff Peischl[3,4], Thomas B. Ryerson[3], Steven S. Brown[3,7], Zachary C.J. Decker[3,4,7], Guillaume Kirgis[3,4], Stephen Conley[8]

[1]Program in Atmospheric and Oceanic Sciences, Princeton University, Princeton, NJ, USA;

[2]NOAA Geophysical Fluid Dynamics Laboratory, Princeton, NJ, USA;

[3]NOAA Earth System Research Laboratory, Boulder, CO, USA;

[4]Cooperative Institute for Research in Environmental Sciences, University of Colorado, Boulder, CO, USA;

[5]Department of Earth and Atmospheric Sciences, University of Houston, Houston, TX, USA;

[6]C&D Technologies Inc., Philadelphia, PA, USA;

[7]Department of Chemistry, University of Colorado, Boulder, CO, USA;

[8]Scientific Aviation Inc., Boulder, CO, USA

Correspondence: Li Zhang (alex.zhang@noaa.gov); Meiyun Lin (meiyun.lin@noaa.gov)

Abstract

The detection and attribution of high background ozone (O_3) events in the southwestern U.S. is challenging but relevant to the effective implementation of the lowered National Ambient Air Quality Standard (NAAQS; 70 ppbv). Here we leverage intensive field measurements from the Fires, Asian, and Stratospheric Transport–Las Vegas Ozone Study (FAST-LVOS) in May–June 2017, alongside high-resolution simulations with two global models (GFDL-AM4 and GEOS-Chem), to pinpoint the sources of O_3 during high-O_3 events. We show stratospheric influence on four out of the ten events with daily maximum 8-hour average (MDA8) surface O_3 above 65 ppbv in the greater Las Vegas region. While O_3 produced from regional anthropogenic emissions dominates pollution in the Las Vegas Valley, stratospheric intrusions can mix with regional pollution to push surface O_3 above 70 ppbv. GFDL-AM4

Atmospheric
Chemistry
and Physics
Discussions
Open Access

EGU

30 captures the key characteristics of deep stratospheric intrusions consistent with ozonesondes, lidar profiles, and co-located measurements of O$_3$, CO, and water vapor at Angel Peak, whereas GEOS-Chem has difficulty simulating the observed features and underestimates observed O$_3$ by ~20 ppbv at the surface. The two models also differ substantially during a wildfire event, with GEOS-Chem estimating ~15 ppbv greater O$_3$, in better agreement with lidar observations. At the surface, the two models bracket the observed MDA8 O$_3$ values during the wildfire event. Both models capture the large-scale transport of Asian

35 pollution, but neither resolves some fine-scale pollution plumes, as evidenced from aerosol backscatter, aircraft, and satellite measurements. U.S. background O$_3$ estimates from the two models differ by 5 ppbv on average and up to 15 ppbv episodically. Our multi-model approach tied closely to observational analysis yields process insights, suggesting that elevated background O$_3$ may pose challenges to achieving a potentially lower NAAQS level (e.g., 65 ppbv) in the southwestern U.S.

40 **Keywords:** background ozone, stratospheric intrusions, wildfires, Asian pollution

1 Introduction

Surface ozone (O$_3$) typically peaks over the high-elevation southwestern U.S. (SWUS) in late spring, in contrast to the summer maximum produced from regional anthropogenic emissions in the low-elevation

45 eastern U.S. (EUS). The springtime O$_3$ peak in the SWUS partly reflects the substantial influence of background O$_3$ from natural sources (e.g., stratospheric intrusions) and intercontinental pollution (Zhang et al., 2008; Fiore et al., 2014; Jaffe et al., 2018). These "non-controllable" O$_3$ sources can contribute ~50 ppbv to mean daily maximum 8-hour average (MDA8) O$_3$ over this region in spring and can episodically push surface O$_3$ to exceed the NAAQS (Lin et al., 2012a; Lin et al., 2012b; Langford et al., 2017).

50 Identifying and quantifying the sources of springtime high-O$_3$ events in the SWUS has been extremely challenging owing to limited measurements, complex topography, and various O$_3$ sources (Langford et al., 2015). As the O$_3$ NAAQS becomes more stringent (lowered from 75 ppbv to 70 ppbv since 2015), quantitative understanding of background O$_3$ sources is of great importance for screening exceptional events, i.e. "…unusual or naturally occurring events that can affect air quality but are not reasonably

55 controllable using techniques that tribal, state or local air agencies may implement…" (U.S. Environmental Protection Agency, 2016). Here we leverage intensive measurements from the 2017 Fires, Asian, and Stratospheric Transport-Las Vegas Ozone Study (FAST-LVOS; Langford et al., manuscript in

preparation), alongside high-resolution simulations with two independent global atmospheric chemistry models (GFDL-AM4 and GEOS-Chem), to characterize the sources of high-O_3 events in the region.

60   Through a process-oriented analysis, we aim to understand the similarities and disparities between these two widely-used global models in simulating O_3 in the SWUS.

Mounting evidence shows that a variety of sources contribute to the high surface O_3 found in the SWUS during spring. For example, observational and modelling studies show that deep stratospheric intrusions can episodically increase springtime MDA8 O_3 levels at high-elevation SWUS sites by 20–40 ppbv

65   (Langford et al., 2009; Lin et al., 2012a). Large-scale transport of Asian pollution across the North Pacific also peaks in spring due to active mid-latitude cyclones and westerly winds, contributing to high-O_3 events and raising mean background O_3 levels over the SWUS (Jacob et al., 1999; Lin et al., 2012b; Lin et al., 2015b; Langford et al., 2017; Lin et al., 2017). Moreover, frequent wildfires add complexity to the study of O_3 in the SWUS (Jaffe et al., 2013; Baylon et al., 2016; Lin et al., 2017; Jaffe et al., 2018). In the late

70   spring and early summer, increased photochemical activity from U.S. domestic anthropogenic emissions can further complicate the unambiguous attribution of observed high-O_3 events in this region to background influence.

Quantifying the contributions of different O_3 sources relies heavily on numerical models. Previous studies, however, have shown large model discrepancies in the estimates of background O_3 in the WUS. Zhang et

75   al. (2011) applied GEOS-Chem to quantify the North American background O_3 (NAB; O_3 that would exist in the absence of North American anthropogenic emissions) during March−August of 2006-2008 and estimated a mean NAB O_3 of 40±7 ppbv at SWUS high-elevation sites, while Lin et al. (2012a) estimated an average of 50±11 ppbv for the late spring to early summer of 2010 with GFDL-AM3. Emery et al. (2012) estimated mean NAB O_3 to be 20−45 ppbv with GEOS-Chem and 25−50 ppbv with CAMx, during

80   spring-summer. Fiore et al. (2014) also showed 10 ppbv differences between GFDL-AM3 and GEOS-Chem in their seasonal average NAB estimates. Previous multi-model studies have largely focused on seasonal mean differences. An event-oriented multi-model comparison, tied closely to intensive field measurements, is needed to provide process insights into the model discrepancy.

Deploying targeted measurements and conducting robust model source attribution are crucial to

85   characterize and quantify the sources of elevated springtime O_3 in the SWUS (Langford et al., 2009; Langford et al., 2012; Lin et al., 2012a; Lin et al., 2012b). This is particularly true for inland areas of the

SWUS, such as greater Las Vegas, where air quality monitoring sites are sparse, making it difficult to assess the robustness of model source attribution (Langford et al., 2015; Langford et al., 2017). Using field measurements from the Las Vegas Ozone Study (LVOS) in May−June 2013 and model simulations,

90 Langford et al. (2017) provided an unprecedented view of the influences of stratosphere-to-troposphere transport (STT) and Asian pollution on the exceedances of surface O_3 in Clark County, Nevada. This study suggests that O_3 descending from the stratosphere and sometimes mingled with Asian pollution can be entrained into the convective boundary layer and episodically brought down to the ground in the Las Vegas area in spring, adding 20−40 ppbv to surface O_3 and pushing MDA8 O_3 above the NAAQS.

95 However, uncertainties remain in previous analyses due to the use of relatively coarse-resolution simulations and limited measurements to connect surface O_3 exceedances at high-elevation baseline sites and low-elevation regulatory sites. High-resolution simulations and more extensive observations are thus needed to further advance our understanding of springtime peak O_3 episodes in the region.

In May−June 2017, the NOAA Earth System Research Laboratory Chemical Sciences Division

100 (NOAA/ESRL CSD) carried out the FAST-LVOS follow up study in Clark County, NV. During this campaign, a broad suite of near-continuous observations was collected by in situ chemistry sensors deployed at a mountain-top site and by state-of-the-art ozone and Doppler lidars located in the Las Vegas Valley. These daily measurements were supplemented by ozonesondes and scientific aircraft flights during four 2 to 4 day long intensive operating periods (IOPs) triggered by the appearance of upper-level

105 troughs above the U.S. West Coast. These extensive measurements, together with high-resolution simulations from two independent global models (GFDL-AM4 and GEOS-Chem), provide us with a rare opportunity to pinpoint the sources of elevated springtime O_3 in the SWUS. We briefly describe the FAST-LVOS field campaign and model configurations in Sect. 2. Following an overall model evaluation (Sect. 3), we present process-oriented analyses of the high-O_3 events from deep stratospheric intrusions,

110 wildfires, regional anthropogenic pollution, and the long-range transport of Asian pollution (Sect. 4). Sect. 5 summarizes differences between the simulated total and background O_3 determined by the two models during FAST-LVOS. Finally, in Sect. 6, the implications of the study are discussed.

2 Measurements and Models

2.1 FAST-LVOS measurement campaign

115   The FAST-LVOS experiment was designed to further our understanding of the impacts of STT, wildfires,
        long-range transport from Asia, and regional pollution on air quality in the Las Vegas Valley. The field
        campaign was carried out between May 17 and June 30, 2017 in Clark County (NV) which includes the
        greater Las Vegas area (Fig. 1). The measurement campaign consisted of daily lidar and in situ
        measurements supplemented by aircraft and ozonesonde profiling during the four IOPs (May 23–25, May

120   31–June 2, June 10–14, and June 28–30). The daily measurements included chemical composition (e.g.,
        CO and O_3) and meteorological parameters (e.g., air temperature and water vapor) recorded with high
        temporal resolution by instruments installed in a mobile laboratory (Wild et al., 2017) parked on the
        summit of Angel Peak (36.32°N, 115.57°W, 2682 m above sea level, a.s.l.), the site of the 2013 LVOS
        field campaign. This mountain-top site, located ~45 km northwest of the Las Vegas City (see Fig. 1), is

125   far from anthropogenic emission sources and mostly receives free tropospheric air during nights, but is
        frequently influenced during the day by air transported from the Las Vegas Valley through upslope flow
        in late spring and summer (Langford et al., 2015). The Tunable Optical Profiler for Aerosols and oZone
        (TOPAZ) 3-wavelength mobile differential absorption lidar (DIAL) system, which was previously
        deployed to Angel Peak during LVOS, was relocated to the North Las Vegas Airport (NLVA, Fig. 1)

130   where it measured 8-minute averaged vertical profiles of O_3 and aerosol backscatter from 27.5 m to ~8
        km above ground level (a.g.l.) with an effective vertical resolution (for O_3) ranging from ~10 m near the
        surface to ~150 m at 500 m a.g.l. and ~900 m at 6 km a.g.l. The aerosol backscatter profiles were retrieved
        at 7.5 m resolution. TOPAZ was operated daily, but not continuously, throughout the campaign. NOAA
        also deployed a continuously operating micro-Doppler lidar at NLVA to measure vertical velocities and

135   relative aerosol backscatter throughout the campaign. Boundary layer heights were inferred from the
        micro-Doppler measurements following the method in Bonin et al. (2018).

        The routine in situ and lidar measurements described above were augmented during the four IOPs by
        ozonesondes launched up to four times per day (30 launches total during the entire campaign) from the
        Clark County Department of Air Quality Joe Neal monitoring site located ~8 km north-northwest of the

140   NLVA. Aircraft measurements were also conducted by Scientific Aviation to sample O_3, methane (CH_4),
        water vapor (H_2O), and nitrogen dioxide (NO_2) between NLVA and Big Bear, CA during the IOPs.
        Readers can refer to our previous studies (Langford et al., 2010; Alvarez II et al., 2011; Langford et al.,
        2015; Langford et al., 2017; Langford et al., 2019) for detailed descriptions and configurations of the

TOPAZ and the other measurement instruments. The FAST-LVOS field campaign is also described in

145   more detail elsewhere (Langford et al., manuscript in preparation).

The FAST-LVOS measurements were augmented by surface O_3 measurements from Joe Neal and other regulatory air quality monitoring sites operated by the Clark County Department of Air Quality (Table S1). Surface observations of O_3 from these and other mostly urban sites were obtained from the U.S. Environmental Protection Agency (EPA) Air Quality System (AQS; https//www.epa.gov/aqs). We

150   average the AQS measurements into 0.5° × 0.625° grids for a direct comparison with model results (as in Lin et al., 2012a, b). Surface observations from rural sites and more representative of background air were obtained from the EPA Clean Air Status and Trends Network (CASTNet; https//www.epa.gov/castnet).

2.2 GFDL-AM4 and GEOS-Chem

AM4 is the new generation of the Geophysical Fluid Dynamics Laboratory chemistry-climate model

155   contributing to the Coupled Model Intercomparison Project, Phase 6 (CMIP6). The model employed in this study, a prototype version of AM4.1 (Horowitz et al., in preparation), differs from the AM4 configuration described in Zhao et al. (2018b, 2018a) by including 49 vertical levels extending up to 1 Pa (~80 km) and interactive stratosphere-troposphere chemistry and aerosols. Major physical improvements to GFDL-AM4, compared to its predecessor GFDL-AM3 (Donner et al., 2011), include a new double-

160   plume convection scheme with improved representation of convective scavenging of soluble tracers, new mountain drag parametrization, and the updated hydrostatic FV^3 cubed-sphere dynamical core (Zhao et al., 2016; Zhao et al., 2018b, a). For tropospheric chemistry, GFDL-AM4 includes improved treatments of biogenic VOCs photo-oxidation, photolysis rates, heterogeneous chemistry, and sulfate and nitrate chemistry and deposition processes (Mao et al., 2013a; Mao et al., 2013b; Paulot et al., 2016; Li et al.,

165   2016; Paulot et al., 2017), as described in more details in Schnell et al. (2018). We implement a stratospheric O_3 tracer (O_3Strat), defined relative to a dynamically varying e90 tropopause (Prather et al., 2011), in GFDL-AM4 to track O_3 originating from the stratosphere (Lin et al., 2012a; Lin et al., 2015a). The model is nudged to NCEP reanalysis winds using a height-dependent nudging technique (Lin et al., 2012b). The nudging minimizes the influences of chemistry-climate feedbacks and ensures that the large-

170   scale meteorological conditions are similar across the sensitivity simulations. We conduct a suite of AM4 simulations at C192 (~50×50 km^2) horizontal resolution for January-June 2017: (1) a BASE simulation with all emissions included; (2) a sensitivity simulation with anthropogenic emissions zeroed out over North America (15°−90°N, 165°−50°W; NAB); (3) a sensitivity simulation with anthropogenic emissions

zeroed out in the U.S. (USB); (4) a sensitivity simulation with Asian anthropogenic emissions shut off,

175   and (5) a sensitivity simulation with wildfire emissions zeroed out (see Table S3). Compared to the NAB simulation, the USB simulation includes additional contributions from Canadian and Mexican anthropogenic emissions. The USB estimates are now generically defined as "background O_3" and used by the U.S. EPA. All the high-resolution simulations are initialized from the C96 (~100×100 km^2) simulations nudged to reanalysis winds from 2009-2016. Over the WUS, the vertical model resolution

180   ranges from ~50−200 m near the surface to ~1−1.5 km near the tropopause and ~2−3 km in much of the stratosphere.

Goddard Earth Observing System coupled with Chemistry (GEOS-Chem; http://geos-chem.org) is a widely-used global chemical transport model (CTM) for simulating atmospheric composition and air quality (Bey et al., 2001; Zhang et al., 2011), driven by assimilated meteorological fields from the NASA

185   Global Modeling and Assimilation Office (GMAO). We used a nested-grid version of GEOS-Chem (v11.01) (Wang et al., 2004; Chen et al., 2009) and conducted high-resolution simulations over North America (10°−70°N, 140°−40°W) at a 0.25° (latitude) × 0.3125° (longitude) horizontal resolution using the GEOS-FP meteorology. Chemical boundary conditions for the nested-grid simulations were provided by GEOS-Chem global simulations at 2° × 2.5° resolution. Key model configurations of GEOS-Chem are

190   listed in Table S2. The model uses a fully coupled NO_X-O_X-hydrocarbon-aerosol-bromine chemistry mechanism in the troposphere ("Tropchem"), whereas a simplified linearized chemistry mechanism (Linoz) is used in the stratosphere to simulate stratospheric ozone and cross-tropopause ozone fluxes (McLinden et al., 2000). Although GEOS-Chem is also equipped with the Universal tropospheric-stratospheric Chemistry eXtension (UCX) mechanism that simulates interactive stratosphere-troposphere

195   chemistry and aerosols (Eastham et al., 2014), this option was not used in the GEOS-Chem simulations presented in this study due to computational constraints. To further save computational resources, we used a reduced vertical resolution of 47 hybrid eta levels as compared to the native 72 levels of GEOS-FP, combining vertical layers above ~80 hPa. The thickness of model vertical layer over the WUS ranges from ~15−100 m near the surface to ~1 km near the tropopause and in the lower stratosphere. Similar GEOS-

200   Chem simulations with simplified treatments of stratospheric chemistry and dynamics have been previously used to estimate background O_3 for U.S. EPA policy assessments (Zhang et al., 2011; Zhang et al., 2014; Fiore et al., 2014; Guo et al., 2018). Thus, it is important to assess the limitation of this model in representing high background O_3 events from stratospheric intrusions. We conduct two simulations

with GEOS-Chem: BASE and a background simulation with anthropogenic emissions zeroed out in the
205 U.S. (Table S3).

2.3 Emissions

Anthropogenic emissions used in GFDL-AM4 are modified from the CMIP6 historical emission inventory
(Hoesly et al., 2018). The CMIP6 emission inventory does not capture the decreasing trend in
anthropogenic NO_X emissions over China after 2011 as inferred from satellite-measured tropospheric NO_2
210 columns (Liu et al., 2016; Fig. S1). We thus scale CMIP6 NO_X emissions over China after 2011 based on
a regional emission inventory developed by Tsinghua University (personal communications with Qiang
Zhang at Tsinghua University; Fig. S1). The adjusted NO_X emission trend over China agrees well with
the NO_2 trend derived from satellite retrievals. We also reduce NO_X emissions over the EUS (25°−50° N,
94.5°−75° W) by 50% following Travis et al. (2016), who suggested that excessive NO_X emissions may
215 be responsible for the common model biases in simulating O_3 over the southeastern U.S. These emission
adjustments reduce mean MDA8 O_3 biases in GFDL-AM4 by ~5 ppbv in spring and ~10 ppbv in summer
over the EUS (Fig. S2). The model applies the latest daily-resolving global fire emission inventory from
NCAR (FINN) (Wiedinmyer et al., 2011), vertically distributed over six ecosystem-dependent altitude
layers from the ground surface to 6 km (Dentener et al., 2006; Lin et al., 2012b). Biogenic isoprene
220 emissions, lightning NO_X emissions, dimethyl sulfide, and sea salt emissions are tied to model
meteorological fields (Donner et al., 2011; Naik et al., 2013).

For GEOS-Chem, anthropogenic emissions over the United States are scaled from the 2011 U.S. NEI to
reflect the conditions in 2017 (https://www.epa.gov/air-emissions-inventories/air-pollutant-emissions-
trends-data). Similar to AM4, we reduce EUS anthropogenic NO_X emissions in GEOS-Chem by 50% to
225 improve simulated O_3 distributions. Anthropogenic emissions over China are based on the 2010 MIX
emission inventory (Li et al., 2017), with NO_X emissions scaled after 2010 using the same trend as in
GFDL-AM4. Biogenic VOC emissions are calculated online with MEGAN (Guenther et al., 2006).
Biomass burning emissions are from the FINN inventory but implemented in the lowest model layer. The
model applies the standard representation of lightning NO_X emissions, with monthly climatology of
230 satellite lightning observations coupled to model deep convection (Murray et al., 2012). The calculation
of lightning NO_X in this study differs from that in Zhang et al. (2014), who used the National Lightning
Detection Network (NLDN) data to constrain model flash rates in the U.S.

Atmospheric
Chemistry
and Physics
Discussions

3 Overall model evaluation

3.1 GFDL-AM4 versus GFDL-AM3

235 We first compare O_3 simulations in AM4 with its predecessor, AM3, which has been extensively used to estimate background O_3 in previous studies (Lin et al., 2012a; Lin et al., 2012b; Fiore et al., 2014; Lin et al., 2015a). Figure 2 shows the comparisons of simulated and observed March mean O_3 vertical profiles and mid-tropospheric O_3 seasonal cycles at the Trinidad Head and Boulder ozonesonde sites. Free tropospheric O_3 measured at both sites in March is representative of background conditions with little

240 influence from U.S. anthropogenic emissions. Thus, we also show O_3 from the NAB simulations with North American anthropogenic emissions zeroed out. As constrained by available AM3 simulations from previous studies, we focus on the 2010-2014 period and compare the NAB estimates as opposed to the USB estimates used in the rest of the paper. Compared with AM3, simulations of free tropospheric O_3 are much improved in AM4. Mean O_3 biases are reduced by 10−25 ppbv in the middle troposphere and 20−65

245 ppbv in the upper troposphere in AM4, reflecting mostly an improved simulation of background O_3 (Fig. 2a). The improvements are most prominent during the cold months (November-April; Fig. 2b), mainly credited to the changes in dynamics/convection schemes in AM4 (Zhao et al., 2018b).

3.2 GFDL-AM4 versus GEOS-Chem

Next, we examine how GFDL-AM4 compares with GEOS-Chem in simulating mean distribution and

250 day-to-day variability of total and USB O_3 in the free troposphere during FAST-LVOS (Fig. 3). Below 700 hPa, total O_3 simulated by the two models often bracket the observed values (Fig. 3a and Fig. S3). Between 700−300 hPa, GFDL-AM4 better captures the observed mean and day-to-day variability of O_3, as evaluated with standard deviation at the Joe Neal ozonesonde site. Further comparison with lidar measurements averaged over 3−6 km altitude above Las Vegas shows that total and USB O_3 in GFDL-

255 AM4 exhibits larger day-to-day variability than in GEOS-Chem (σ = 8.1 ppbv in observations, 8.1 ppbv in AM4, and 6.7 ppbv in GEOS-Chem; Fig.3c). For mean O_3 levels in the free troposphere, AM4 estimates a 7 ppbv contribution from U.S. anthropogenic emissions (total O_3 minus USB), while GEOS-Chem suggests only 3.5 ppbv. The largest discrepancies between the two models occurred during a stratospheric intrusion event on June 11−13 (the blue shaded period in Fig. 3c). During this period, AM4 simulates

260 elevated O_3 (70−75 ppbv) broadly consistent with the lidar and sonde measurements, while GEOS-Chem considerably underestimates the observations by 20 ppbv. Consistent with total O_3, USB O_3 in GFDL-

Atmospheric
Chemistry
and Physics

Discussions

Open Access

EGU

AM4 is much higher than GEOS-Chem during the STT periods. The two models also differ substantially in total O_3 and USB estimates in late June. Differences in the two models during these two periods will be discussed in more detail in Sect. 4.

265 **4 Process-oriented analysis of high-ozone events during FAST-LVOS**

We identify ten events with observed MDA8 O_3 exceeding 65 ppbv at multiple sites in the greater Las Vegas area during April–June 2017. Table 1 provides an overview of the events, the dominant source for each event, the surface sites impacted, and associated analysis figures presented in this article. Specifically, we conduct detailed analyses for several events occurring during the FAST-LVOS campaign period (May 270 20–June 30): including the previously mentioned deep STT event during June 11–14, a regional anthropogenic pollution event on June 16, a wildfire event on June 22, an Asian pollution event on May 24, and an event on June 28 that could not be clearly linked to any of the above O_3 sources. We begin in Sect. 4.1 by examining the O_3/CO relationships and collocated meteorological conditions using the high temporal resolution measurements from the NOAA/ESRL mobile lab deployed at Angel Peak. Then, in 275 Sect. 4.2–4.6, we analyze the temporal evolution and vertical profiles of O_3 above Las Vegas during each event using lidar and ozonesonde measurements and examine how well GFDL-AM4 and GEOS-Chem simulate the observed high-O_3 layers. Furthermore, we investigate the spatial distributions of surface MDA8 O_3 from observations and model simulations to identify the areas impacted by each event and to provide quantitative O_3 source attributions for each event.

280 **4.1 Observed $O_3/CO/H_2O$ relationships**

Relationships between concurrently measured O_3 and CO are useful to identify the possible origins of elevated surface O_3 (Parrish et al., 1998; Herman et al., 1999; Langford et al., 2015). During FAST-LVOS, in-situ 1-min measurements at Angel Peak show significant differences in $\Delta O_3/\Delta CO$ and water vapor content between air plumes during a variety of events (Figs. 4–5). Notably, on June 11, O_3 was negatively 285 correlated with CO ($\Delta O_3/\Delta CO$ = -3.79). This anti-correlation is distinctly different from the O_3/CO relationships during other periods (e.g., $\Delta O_3/\Delta CO$ = 0.68–0.70 on June 16 or $\Delta O_3/\Delta CO$ = 1.08 on June 2). The negative correlation (high O_3 together with low CO) serves as a strong evidence of a stratospheric origin of the air masses on June 11, since O_3 is much more abundant in the stratosphere than in the troposphere whereas CO is mostly concentrated within the troposphere where it is directly emitted or

290   chemically formed (Langford et al., 2015). On the contrary, simultaneously elevated O_3 and CO suggests influences by wildfires (e.g., June 22) or anthropogenic (e.g., June 16) pollution (Figs. 5b−d and S4). In particular, the exceptionally high CO levels (~100−440 ppbv) and elevated O_3 on June 22 (Fig. 5e) suggest influences from wildfires, but the poor correlation between CO and O_3 may imply mixings of other sources of plumes (e.g., urban pollution).

295   We gain further insights by examining water vapor concurrently measured at Angel Peak. Air masses from the lower stratosphere are generally dry, whereas wildfire/urban plumes from the near-surface layer are relatively moist (Langford et al., 2015). Thus, the dry conditions of the air masses on June 11 support our conclusion that the plume was from the lower stratosphere and transported downward to Angel Peak (Fig. 5a). These conditions are in contrast to those of the urban/wildfire plumes transported from the Las Vegas

300   Valley (Figs. 5). Additionally, we separate the anthropogenic plumes on June 16 into daytime and nighttime conditions because of a diurnal variation of air conditions (relatively dry at night versus wet during daytime; Figs. 5c−d). This analysis further demonstrates that the anthropogenic pollution plume during nighttime is wetter than the stratospheric air on June 11. On June 14, measured O_3 was positively correlated with CO but with lower levels of water vapor than those in regional pollution and wildfire

305   plumes, suggesting that the stratospheric air which reached Angel Peak earlier may have been mixed with local pollution. On June 28, O_3 was positively correlated with CO and the air masses were relatively dry (Figs. 5f), indicating that the plume was likely from aged pollution transported from Asia or Southern California as opposed to from fresh pollution from the Las Vegas Valley. Identifying the primary source of the high-O_3 events solely based on observations is challenging; additional insights from models are

310   thus needed as we demonstrate below.

4.2 Characteristics of stratospheric intrusion during June 11−14

Analysis of the 250 hPa potential vorticity and the AM4 model stratospheric O_3 tracers shows that significant stratospheric influence (up to 40 ppbv) on surface O_3 in the SWUS occurred on April 22−23, May 13−14, and June 11−14 (Table 1; Figs. S5−S6). Below, we focus on the June 11−14 event, which

315   was the subject of a 4-day FAST-LVOS IOP with 60 hours of continuous O_3 lidar profiling and 13 ozonesonde launches, in addition to continuous in situ measurements at Angel Peak.

Deep stratospheric intrusion on June 11−12

Synoptic-scale patterns of potential vorticity (PV) indicate a strong mid-latitude cyclone over the northwest U.S. on June 12 (PV = 4–5 PVU in Fig. 6a). The PV pattern displays a "hook-shaped" streamer
320 of air extending from the northern U.S. to the Intermountain West, a typical feature for a STT event (Lin et al., 2012a; Akritidis et al., 2018). This upper-level trough penetrated southeastwardly towards the SWUS, facilitating the descent of stratospheric air masses into the lower troposphere. Ozonesondes launched at Joe Neal on June 12 recorded elevated O_3 levels of 150–270 ppbv at 5–8 km altitude (color-coded circles in Fig. 6b). Consistent with the ozonesonde measurements, GFDL-AM4 shows that O_3-rich
325 stratospheric air masses descended isentropically towards the study region, with simulated O_3 reaching 90 ppbv at ~2 km altitude (Fig. 6b). For comparison, GEOS-Chem simulates a much weaker and shallower intrusion.

TOPAZ lidar measurements at NLVA vividly characterize the strength and vertical depth of intruding O_3 tongues evolving with time (Fig. 7a). A tongue of high O_3 exceeding100 ppbv descended to as low as 2–3
330 km altitude on June 12. GFDL-AM4 captures both the timing and structure of the observed high-O_3 layer and attributes it to a stratospheric origin as supported by the model stratospheric O_3 tracer. In contrast, GEOS-Chem substantially underestimates the depth and magnitude of the observed high-O_3 layers in the free troposphere. Zhang et al. (2014) also showed that GEOS-Chem captures the timing of stratospheric intrusions but underestimates their magnitude by a factor of 3.

335 *Mixing of stratospheric ozone with regional pollution on June 14*

Stratospheric air masses that penetrate deep into the troposphere can mix with regional anthropogenic pollution and gradually lose their typical stratospheric characteristics (cold and dry air containing low levels of CO), challenging diagnosis of stratospheric impacts based directly on observations (Cooper et al., 2004; Lin et al., 2012b; Trickl et al., 2016). On June 14, O_3 measured at Angel Peak is positively
340 correlated with CO ($\Delta O_3/\Delta CO$ = 0.75; Fig. 5b), similar to conditions of anthropogenic pollution on June 26 (Fig. 5c–d). However, observed $\Delta O_3/\Delta NOz$ in the plume (11.4) was much larger than those (~1–7) of typical urban plumes (Kleinman et al., 2002). TOPAZ lidar shows elevated O_3 of 70–80 ppbv concentrated within the boundary layer below 3 km altitude (Fig. 7b). GFDL-AM4 captures the observed O_3 enhancements within the PBL and estimates a stratospheric contribution of 20–30 ppbv (30% of the total),
345 suggesting that O_3 from the deep stratospheric intrusion on the previous days had been mixed with regional anthropogenic pollution to elevate O_3 in the PBL on June 14. GEOS-Chem is unable to simulate the

observed features. This case study demonstrates the value of integrating observational and modeling analysis for the attribution of high-O_3 events over a region with complex O_3 sources.

Influence on surface ozone

350   We next evaluate to what extent the stratospheric intrusion affected surface O_3 across the western U.S. during June 11−14 (Fig. 8). Observations show that high MDA8 O_3 exceeding 60 ppbv first emerged on June 11 over Southern Nevada, consistent with the arrival of stratospheric air masses as inferred from the negative correlation between O_3 and CO measured at Angel Peak (Fig. 5a). Over the next few days, the areas with observed MDA8 O_3 approaching 70 ppbv gradually shifted southward from Nevada and

355   Colorado to Arizona and New Mexico. By June 13−14, observed surface MDA8 O_3 exceeded 70 ppbv over a large proportion of the WUS, including the Phoenix area. GFDL-AM4 captures well the observed day-to-day variability of high-O_3 spots over the WUS, although the model overall has high biases. Over the areas where observed MDA8 O_3 levels are 60−75 ppbv, GFDL-AM4 estimates 50−65 ppbv USB O_3 with simulated stratospheric O_3 accounting for 30−40 ppbv at the surface (not shown). In contrast, GEOS-

360   Chem underestimates observed surface MDA8 O_3 by 10−20 ppbv during this event and estimates only 40−55 ppbv USB (Fig. 8). These results are consistent with the fact that GEOS-Chem does not capture the structure and magnitude of deep stratospheric intrusions during the period (Figs. 3, 6, and 7) possibly due to the simplified treatments of stratospheric chemistry and dynamics (Sect. 2.3).

The extent to which stratospheric intrusions contribute to surface O_3 at low-elevation sites over the WUS

365   is poorly characterized in previous studies. Notably, surface O_3 at three low-elevation (~700−800 m a.s.l.) air quality monitoring sites in Clark County exceeded the current NAAQS level of 70 ppbv on June 14: 74 ppbv at Joe Neal, 73 ppbv at North Las Vegas Airport, and 71 ppbv at Walter Johnson. The number of monitoring sites with O_3 exceedances would have increased to eleven in Clark County if the NAAQS had been lowered to 65 ppbv. While O_3 produced from regional anthropogenic emissions still dominates

370   pollution in the Las Vegas Valley (Fig. S7), our analysis shows that stratospheric intrusions can mix with regional pollution to push surface O_3 above the NAAQS.

4.3 Wildfires on June 22

The lidar measurements at NLVA from June 22 show broad O_3 enhancements from the surface to 4 km altitude (Fig. 9a). The Angel Peak measurements (~3 km altitude) meanwhile detected elevated CO

375   (~100–440 ppbv) and a collocated O_3 enhancement in warm and moist air masses, suggesting that wildfire

plumes were transported into the region (Fig. 5e). Significant enhancements in aerosol backscatter were

observed above NLVA (3–6 km altitude), confirming the presence of wildfire smoke (see Sect. 4.6). After

12:00 PDT (19:00 UTC), a deep PBL (3–4 km) developed. O_3 within the PBL was significantly enhanced

(> 80 ppbv) in the afternoon, likely due to strong O_3 production through reactions between abundant VOCs

380   in the wildfire plumes and NO_X in urban environments (Singh et al., 2012; Gong et al., 2017). Surface

MDA8 O_3 exceeded 70 ppbv at multiple sites in the Las Vegas Valley during the event (Table 1).

Unfortunately, the synoptic conditions did not trigger an IOP, so there was no aircraft or ozonesonde

measurement during this event.

GFDL-AM4 fails to capture the O_3-rich plumes above Clark County on June 22 (Fig. 9a). GEOS-Chem

385   captures the high-O_3 layers within the PBL but overestimates observed O_3 by 10–15 ppbv at 3–6 km

altitude, as compared with lidar measurements at NLVA (Figs. 3b and 9a), likely due to excessive O_3 from

lightning NO_X over the southern U.S. (Zhang et al., 2011; Zhang et al., 2014). At the surface, total O_3

simulated by the two models bracket the observed values at sites in the Las Vegas area and across the

Intermountain West, with GEOS-Chem estimating 10–15 ppbv greater contribution from USB in the

390   Southwest (Fig. 10a). Overall, GEOS-Chem simulations during this wildfire event seem to be more

consistent with observations than GFDL-AM4. However, we cannot rule out the possibility that the better

agreement between observation and GEOS-Chem simulations during this event may reflect excessive O_3

from lightning NO_X in the model.

Meteorological conditions (e.g., temperature and wind fields) on June 22 in the reanalysis data used by

395   GFDL-AM4 and GEOS-Chem are very similar over the WUS (not shown). The two models use the same

wildfire emissions (FINN) but with different vertical distributions. Fire emissions are distributed between

the surface and 6 km altitude in GFDL-AM4 but are placed at the surface level in GEOS-Chem. We

conduct several sensitivity simulations with GFDL-AM4 to investigate the causes of the model biases.

Placing all fire emissions at the surface in GFDL-AM4 results in ±5 ppbv differences in modeled MDA8

400   O_3 on June 22 (Fig. S8). Observations suggested that 40% of NO_X can be converted rapidly to PAN and

20% to HNO_3 in fresh boreal fire plumes over North America (Alvarado et al., 2010). Both models

currently treat 100% of wildfire NO_X emissions as NO. We conduct an additional AM4 sensitivity

simulation, in which 40% of the wildfire NO_X emissions are released as PAN and 20% as HNO_3. This

treatment results in ±2 ppbv differences in simulated monthly mean MDA8 O_3 during an active wildfire

405   season (August 2012; Fig. S9). Future efforts are needed to investigate the ability of current models to simulate O_3 formations in fire plumes (Jaffe et al., 2018).

4.4 Regional anthropogenic pollution event on June 16

Regional and local anthropogenic emissions were important sources of elevated O_3 in Clark County during FAST-LVOS, contributing to three out of ten observed high-O_3 events above 65 ppbv during April–June

410   2017 (Table 1). Below, we focus on the June 16 event when severe O_3 pollution with MDA8 O_3 exceeding 70 ppbv occurred over California, Arizona, parts of Nevada, and New Mexico (analysis on the other two events are shown in Figs. S10–S11). The TOPAZ lidar measurements show an elevated O_3 layer at ~3 km altitude until midday and high O_3 (up to 90 ppbv) in the 4-km–deep PBL (Fig. 9b). However, this event did not trigger an IOP, so ozonesonde and aircraft measurements are unavailable. Both GFDL-AM4 and

415   GEOS-Chem capture the buildup of O_3 pollution in the PBL (Fig. 9b) and the spatial pattern of MDA8 O_3 enhancements at the surface across the SWUS (Fig. 10b). With a higher horizontal resolution, GEOS-Chem better resolves the structure of the O_3 pollution plume for this event. Both models show boundary layer O_3 enhancements in total O_3 simulations but not in USB simulations (Fig. 9b), indicating that regional or local anthropogenic emissions are the dominant source of observed high-O_3 levels on June 16

420   (contributing 20–30 ppbv). The model attribution to U.S. emissions is consistent with the positive correlation between O_3 and CO measured at Angel Peak (Fig. 5c–5d).

4.5 Long-range transport of Asian pollution on May 20–24

During May 20–24, long-range transport of Asian pollution toward the WUS was observed via large-scale CO column observations with Atmospheric Infrared Sounder (AIRS) on NASA's Aqua satellite (Fig. 11a).

425   These Asian plumes spent a few days travelling eastward across the Pacific and reached the west coast of the U.S. on May 23 during the first FAST-LVOS IOP (May 23–25). The lidar measurements at NLVA on May 24 clearly showed high-O_3 plumes (> 70 ppbv) concentrated within the layers of 1–4 km and 6–8 km altitude above the Las Vegas Valley throughout the day (Fig. 12a). The descending O_3 plumes reached the top of the PBL (~1.5 km altitude) at 11:00 PDT (18:00 UTC) and were later mixed into the growing

430   PBL (up to 4 km altitude), contributing to the elevated surface O_3. Meanwhile, MDA8 O_3 approached or exceeded the 70-ppbv NAAQS at multiple sites in California, Idaho, Wyoming, and Nevada (Fig. 13a), suggesting that there were large-scale surface O_3 enhancements over the WUS due to Asian pollution.

Compared with observations, both GFDL-AM4 and GEOS-Chem capture the observed O_3-rich plumes at surface–4 km and 6–8 km altitude in Clark County and the elevated surface O_3 levels over the WUS

435   during the event. Background simulations with both models suggest that USB O_3 substantially contributed to the high-O_3 layers above the Las Vegas Valley (USB = 50–60 ppbv in GFDL-AM4 and 60–80 ppbv in GEOS-Chem). These results indicate that both models are capable of capturing large-scale Asian pollution plumes.

Sensitivity simulations with GFDL-AM4 further suggest that Asian pollution contributes 6–10 ppbv to

440   surface O_3 in the high-O_3 regions over the WUS (Fig. 13a). Meanwhile, at low-elevation sites in Clark County, average O_3 enhancement from Asian pollution is estimated to be ~7 ppbv (Fig. S7e), quantitatively close to the estimates (up to 10 ppbv) by Langford et al. (2017) during an event in late May 2013. This model-estimated Asian O_3 enhancement is comparable to the contribution from U.S. anthropogenic emissions (~10 ppbv; calculated as total O_3 minus USB with GFDL-AM4), possibly

445   contributing to the high surface O_3 events measured on May 24 at several high-elevation sites such as Arden Peak (72 ppbv) and Yosemite National Park (70 ppbv) in the SWUS. It is also worth noting that during this event, MDA8 O_3 at four surface sites in Clark County was below 70 ppbv but above 65 ppbv. Thus, more exceedances would have occurred if the level for the NAAQS were lowered to 65 ppbv.

4.6 An unattributed event: June 28

450   The lidar measurements from June 28 show a fine-scale structure with a narrow O_3 layer exceeding 100 ppbv at 3–4 km altitude during 08:00–14:00 PDT (15:00–21:00 UTC shown in Fig. 12b). An ozonesonde launched at 12:00 PDT (not shown) also detected a high-O_3 layer (~115 ppbv) between 3.5 and 4 km altitude. This high-O_3 filament appears to descend and mix into the PBL after 14:00 PDT (21:00 UTC), contributing to elevated O_3 within the PBL in the afternoon. Both models have difficulties simulating the

455   observed high-O_3 layer at 3–4 km altitude and the enhanced O_3 levels within the PBL during this event (Fig. 12b). We, therefore, focus on available airborne and in situ measurements to investigate the origin of this O_3 filament.

Our examinations of large-scale satellite CO column measurements reveal a migration of high-CO plumes during June 23–27 from Asia that arrived at the west coast of the U.S. on June 27 (Fig. 11b). GFDL-AM4

460   reveals elevated contributions from Asian pollution over the WUS on June 28 (5–6 ppbv; Figs. 13b),

Atmospheric
Chemistry
and Physics
Discussions

although the model underestimates the observed O_3. Aircraft measurements above the Las Vegas Valley showed collocated enhancements in CH_4 and O_3 coincident with free tropospheric water vapor values within the high-O_3 filament at 3–4 km altitude (Fig. 14b). In-situ measurements at Angel Peak show concurrent increases in CO and O_3 coincident with relatively dry conditions (Figs. 5f). These observations

465   indicate that the O_3-rich plume appears to be unrelated to stratospheric intrusions. Aerosol backscatter measurements at NLVA show only a very slight enhancement in backscatter within the elevated O_3 layer on June 28, in contrast to the thick smoke observed on June 22 influenced by fresh wildfires in the Las Vegas Valley (Fig. 14). Overall, our analyses presented here suggest that the most likely sources for this high-O_3 filament on June 28 are aged fire plumes or fine-scale Asian pollution plume, although the lofting

470   of pollution above Southern California followed by transport into the free troposphere over Las Vegas cannot be ruled out (Langford et al., 2010). HYSPLIT and FLEXPART analyses presented in Langford et al., (in preparation) suggest a possible connection to the Schaeffer Fire (https://en.wikipedia.org/wiki/Schaeffer_Fire) in the Sequoia National Forest in California. This event further demonstrates the complexity of O_3 sources in the SWUS. We recommend measurements of

475   atmospheric compounds like acetonitrile (CH_3CN, abundant in fire plumes) and methyl chloride (CH_3Cl, abundant in Asian pollution) (Holzinger et al., 1999; Barletta et al., 2009) via aircraft and in situ platforms in future field campaigns in the region to help identifying the sources of such high-O_3 filaments.

5 Comparison of background ozone simulated with GFDL-AM4 and GEOS-Chem

Here, we summarize the differences in total and background O_3 between the two models over the WUS.

480   Figure 15 shows the times series of observed and simulated O_3 at four high-elevation sites and one low-elevation site in the region during the study period. Notably, STT events (highlighted in blue shading) occurred frequently during April–June with MDA8 O_3 exceeding or approaching the current NAAQS of 70 ppbv. Compared with observations, GFDL-AM4 captures the spikes of MDA8 O_3 during STT events associated with elevated USB O_3 and stratospheric O_3 (e.g., April 23, May 13, and June 11). During these

485   events, GEOS-Chem significantly underestimates observed O_3 by 10–25 ppbv and simulates much lower USB O_3 levels than GFDL-AM4, since the model underestimates the magnitude of STT (Sect. 4.2). The two models also differ substantially in total and USB O_3 (14–18 ppbv) during the June 22 wildfire event (yellow shading), with GEOS-Chem overestimating observations at high-elevation sites while GFDL-AM4 underestimating observations at both high- and low-elevation sites. It is also worth noting that more

490   exceedances would have occurred at these sites if a standard of 65 ppbv were implemented (dotted lines

in Fig. 15). The O_3 standard-exceeding rate in Clark County would have increased by 3–4 times during late spring to early summer given a 65-ppbv O_3 NAAQS (e.g., increased from 2.4% to 10.8% in 2017; Fig. S12).

GFDL-AM4 and GEOS-Chem differ in the spatial distributions and magnitudes of April–June mean USB O_3 at the surface and in the free troposphere over the U.S. (Fig. 16). USB O_3 in GFDL-AM4 peaks over the high-elevation Intermountain West at the surface (45−55 ppbv) and over the northern U.S. in the free troposphere (3−6 km altitude; 50−65 ppbv) due to the influence of STT. In comparison, GEOS-Chem simulates higher USB O_3 levels in southwestern states (e.g., Texas), both at the surface (45−50 ppbv) and at 3−6 km altitude (55−65 ppbv), likely due to excessive lightning NO_X during early summer (Zhang et al., 2011; Zhang et al., 2014). These discrepancies in USB between the two models likely reflect that GFDL-AM4 simulates stronger STT influences over the WUS while it produces less O_3 from weaker lightning NO_X emissions in the free troposphere over the southern U.S. than GEOS-Chem (Fiore et al., 2014). Despite a quantitative disparity, both models simulate higher USB O_3 levels over the WUS (45−55 ppbv in GFDL-AM4 and 35−45 ppbv in GEOS-Chem) than over the EUS at the surface (Fig. 16a). Our USB O_3 estimates with GEOS-Chem are generally consistent with the USB estimates reported by Zhang et al. (2011) for 2006−2008 and by Guo et al. (2018) for 2004−2012. A few earlier studies have quantified NAB O_3 by zeroing out North American anthropogenic emissions (Zhang et al., 2011; Lin et al., 2012a; Fiore et al., 2014; Zhang et al., 2014). USB O_3 estimates in our study include the additional contribution from Canadian and Mexican emissions. USB O_3 at Clark County sites is ~4 ppbv greater than NAB O_3 estimated by the same GFDL-AM4 model (Table S4). We also find that NAB O_3 estimated with the new GFDL-AM4 model is ~5 ppbv lower than the NAB estimates by its predecessor GFDL-AM3 (Lin et al., 2012a; Lin et al., 2017) for the WUS during March−April (Fig. S13), consistent with an improved simulation of free tropospheric ozone in AM4 during spring (Fig. 2). During early summer, the NAB O_3 levels estimated by AM3 and AM4 are similar (Fig. S13).

We further compare simulated surface MDA8 O_3 against observations at 12 high-elevation sites (> 1500 m altitude; 11 CASTNet sites and the Angel Peak site as encircled in black in Fig. 1 and listed in Table S1) in the WUS (Fig. 17). As shown, observed high-O_3 events (MDA8 O_3 > 65 ppbv) in the WUS are generally associated with enhanced background O_3 in both models (USB O_3 = 50–60 ppbv in GFDL-AM4 or 45–55 ppbv in GEOS-Chem; Fig. 17a). Many of the standard-exceeding O_3 events during April–June

520   at these high-elevation sites appear to be related to stratospheric intrusions (Fig. S14). Overall, GFDL-AM4 better captures the high-O_3 events influenced by elevated background O_3 contributions, whereas GEOS-Chem underestimates observed O_3 during the extreme events (MDA8 $O_3 > 70$ ppbv). For mean MDA8 O_3 at these sites, GFDL-AM4 is biased high by 3 ppbv while GEOS-Chem is biased low by 5 ppbv. A recent study by Lin et al. (2019) found that an improved treatment of ozone dry deposition can

525   reduce mean springtime ozone biases in GFDL-AM4 by 5 ppbv. Mean USB O_3 simulated with GFDL-AM4 is 51.4±7.8 ppbv at these sites, higher than that in GEOS-Chem (45.7±5.7 ppbv; Fig. 17b). Probability distributions show that GFDL-AM4 simulates a wider range of total and USB O_3 than GEOS-Chem, reflecting relative skill in capturing the day-to-day variability of O_3 (Fiore et al., 2014). Supporting the conclusions of Lin et al. (2015b), our simulations with GFDL-AM4 for 2010–2017 also show strong

530   year-to-year variability in WUS background O_3, with STT as the major contributor (Table S4). May–June mean USB MDA8 O_3 estimates at Clark County sites are 50.9 ppbv in 2017, slightly lower than the 2010-2017 average of 52.3±2.0 ppbv.

6 Conclusions

Through a process-oriented analysis of intensive measurements from the 2017 FAST-LVOS field

535   campaign and high-resolution simulations with two independent global models (GFDL-AM4 and GEOS-Chem), we pinpoint the sources of observed MDA8 O_3 above 65 ppbv in the SWUS. We identify the high-O_3 events associated with stratospheric intrusions (April 22–23, May 13–14, and June 11–14), regional anthropogenic pollution (June 2, June 16, and June 29–30), wildfires (June 22 and possibly June 28), and Asian pollution (May 24) in the study period. During a deep intrusion event (June 11–14), coincident

540   measurements of O_3, CO, and meteorological parameters by the NOAA mobile lab at Angel Peak show a sharp increase in O_3 coinciding with a decrease in CO and water vapor, a marker for air of stratospheric origin. These characteristics are in contrast to the concurrent increases in O_3 and CO in humid and warm urban plumes and wildfires plumes transported from the Las Vegas Valley. We suggest these observation-based indicators can produce a useful first guess of the origin of high-O_3 events in the SWUS.

545   During the STT event, ozonesonde and lidar measurements clearly show high-O_3 plumes descending to ~3 km altitude above Las Vegas. Transported stratospheric O_3 reached high-elevation sites across the Intermountain West during June 11–13 and was then mixed with regional pollution on June 14, contributing ~30 ppbv to surface O_3 and pushing observed MDA8 O_3 to approach or exceed 70 ppbv at

multiple sites in the Las Vegas Valley. GFDL-AM4 captures the observed layered features of stratospheric

550 intrusions well; GEOS-Chem, with simplified stratospheric chemistry and dynamics, is unable to simulate these features and underestimates surface O_3 by 20 ppbv during this event (Figs. 6−8). On June 22, wildfires were likely mixed with regional emissions and contributed to increased surface O_3 (Figs. 9−10). During this event, the two models also differ substantially in total and background O_3 simulations, with GEOS-Chem estimating ~15 ppbv greater O_3, in better agreement with lidar observations. At the surface,

555 the two models bracket the observed MDA8 O_3 values during the wildfire event. Long-range transport of Asian pollution is estimated to have a noticeable contribution to surface O_3 (6−10 ppbv) on May 24, and both models capture the large-scale transport of Asian plumes during the event. However, neither model is able to resolve the fine-scale high-O_3 filaments on June 28 which was likely attributable to small-scale fire smoke transported from California or pollution from Asia, as evidenced by observational analysis

560 (Figs. 11−14). This multi-model approach tied closely to intensive measurements provides insights into the capability and uncertainty of models in total and background O_3 estimates and harnesses the strengths of individual models to characterize the sources of high-O_3 events.

Both GFDL-AM4 and GEOS-Chem estimate substantial background contributions to surface O_3 during late spring to early summer in 2017 over the SWUS (45−55 ppbv in GFDL-AM4 and 35−45 ppbv in

565 GEOS-Chem). The two models have a disparity of ~5 ppbv on average in estimating USB O_3 over the SWUS (Figs. 16−17). Specifically, the two models simulate different spatial patterns of USB O_3 in the free troposphere, with GFDL-AM4 estimating higher levels in the northwestern U.S. from STT contributions while GEOS-Chem simulating a higher background level over the southwestern U.S. from more abundant lightning NO_X. Our event-oriented analyses show that the two models differ significantly

570 in USB O_3 simulations during STT and wildfire events, both at the surface and within the free troposphere (Figs. 3 and 7−10). Discrepancies in surface USB O_3 between the two models are as large as ~15 ppbv during these events. Model differences in dynamics, chemistry, and biogenic emissions of ozone precursors may also contribute to differences in background O_3 simulations. Future efforts concerning these aspects are needed to further our understanding of background O_3 estimates in the models.

575 This study presents a detailed analysis of the sources of high background O_3 events over the SWUS, contributing to the current understanding of the springtime O_3 peak in this region. As suggested in the FAST-LVOS study, stratospheric intrusions, Asian pollution, and wildfires are important sources of the observed springtime high-O_3 events above 65 ppbv in the SWUS, and many more exceedances would

have occurred in the region if the NAAQS had been lowered to 65 ppbv. Although the transport of Asian

580   pollution will possibly decline as a result of decreasing emissions in Asia in recent years (Liu et al., 2016), the increasing frequency of wildfires under a warming climate (e.g., Westerling et al., 2006; Dennison et al., 2014) and growing global methane levels (e.g., West et al., 2006; Morgenstern et al., 2013) would likely foster higher background O_3 levels in the coming decades (Lin et al., 2017). These potentially increasing background O_3 sources, together with natural stratospheric intrusions, will leave little margin

585   for anthropogenic O_3 from local and regional formation/transport, making it difficult for state and local agencies to meet current or potentially tightened O_3 NAAQS in the SWUS through domestic emissions reductions.

Data availability. Model simulations presented in this manuscript are available upon request

590   (alex.zhang@noaa.gov). Field measurements during FAST-LVOS are available at https://www.esrl.noaa.gov/csd/projects/fastlvos.

Author contributions. MYL conceived this study and designed the model experiments; LZ performed the GFDL-AM4 simulations and all analysis under the supervision of MYL; EK and YXW conducted the GEOS-Chem simulations; LWH and YXW assisted in the interpretation of model results; AOL, CJS, RJA,

595   IP, PC, JP, TBR, SSB, ZCJD, GK, and SC carried out field measurements. LZ and MYL wrote the article with inputs from all coauthors.

Competing interests. The authors declare that they have no conflict of interest.

Disclaimer. The statements, findings, and conclusions are those of the author(s) and should not be construed as the views of the agencies.

Atmospheric
Chemistry
and Physics
Discussions

610

References

Akritidis, D., Katragkou, E., Zanis, P., Pytharoulis, I., Melas, D., Flemming, J., Inness, A., Clark, H., Plu, M., and Eskes, H.: A deep stratosphere-to-troposphere ozone transport event over Europe simulated in CAMS global and regional forecast systems: analysis and evaluation, Atmos. Chem. Phys., 18,
615   15515-15534, https://doi.org/10.5194/acp-18-15515-2018, 2018.

Alvarado, M. J., Logan, J. A., Mao, J., Apel, E., Riemer, D., Blake, D., Cohen, R. C., Min, K. E., Perring, A. E., Browne, E. C., Wooldridge, P. J., Diskin, G. S., Sachse, G. W., Fuelberg, H., Sessions, W. R., Harrigan, D. L., Huey, G., Liao, J., Case-Hanks, A., Jimenez, J. L., Cubison, M. J., Vay, S. A., Weinheimer, A. J., Knapp, D. J., Montzka, D. D., Flocke, F. M., Pollack, I. B., Wennberg, P. O.,
620   Kurten, A., Crounse, J., Clair, J. M. S., Wisthaler, A., Mikoviny, T., Yantosca, R. M., Carouge, C. C., and Le Sager, P.: Nitrogen oxides and PAN in plumes from boreal fires during ARCTAS-B and their impact on ozone: an integrated analysis of aircraft and satellite observations, Atmos. Chem. Phys., 10, 9739-9760, https://doi.org/10.5194/acp-10-9739-2010, 2010.

Alvarez II, R. J., Senff, C. J., Langford, A. O., Weickmann, A. M., Law, D. C., Machol, J. L., Merritt, D.
625   A., Marchbanks, R. D., Sandberg, S. P., Brewer, W. A., Hardesty, R. M., and Banta, R. M.: Development and Application of a Compact, Tunable, Solid-State Airborne Ozone Lidar System for Boundary Layer Profiling, Journal of Atmospheric and Oceanic Technology, 28, 1258-1272, https://doi.org/10.1175/jtech-d-10-05044.1, 2011.

Barletta, B., Meinardi, S., Simpson, I. J., Atlas, E. L., Beyersdorf, A. J., Baker, A. K., Blake, N. J., Yang,
630   M., Midyett, J. R., Novak, B. J., McKeachie, R. J., Fuelberg, H. E., Sachse, G. W., Avery, M. A., Campos, T., Weinheimer, A. J., Rowland, F. S., and Blake, D. R.: Characterization of volatile organic compounds (VOCs) in Asian and north American pollution plumes during INTEX-B: identification of specific Chinese air mass tracers, Atmos. Chem. Phys., 9, 5371-5388, https://doi.org/10.5194/acp-9-5371-2009, 2009.

635 Baylon, P. M., Jaffe, D. A., Pierce, R. B., and Gustin, M. S.: Interannual Variability in Baseline Ozone and Its Relationship to Surface Ozone in the Western U.S, Environ. Sci. Technol., 50, 2994-3001, https://doi.org/10.1021/acs.est.6b00219, 2016.

Bey, I., Jacob, D. J., Yantosca, R. M., Logan, J. A., Field, B. D., Fiore, A. M., Li, Q., Liu, H. Y., Mickley, L. J., and Schultz, M. G.: Global modeling of tropospheric chemistry with assimilated meteorology:
640   Model description and evaluation, J. Geophys. Res.-Atmos., 106, 23073-23095, https://doi.org/10.1029/2001JD000807, 2001.

Bonin, T. A., Carroll, B. J., Hardesty, R. M., Brewer, W. A., Hajny, K., Salmon, O. E., and Shepson, P. B.: Doppler Lidar Observations of the Mixing Height in Indianapolis Using an Automated Composite Fuzzy Logic Approach, Journal of Atmospheric and Oceanic Technology, 35, 473-490,
645   https://doi.org/10.1175/jtech-d-17-0159.1, 2018.

Chen, D., Wang, Y., McElroy, M. B., He, K., Yantosca, R. M., and Le Sager, P.: Regional CO pollution and export in China simulated by the high-resolution nested-grid GEOS-Chem model, Atmos. Chem. Phys., 9, 3825-3839, https://doi.org/10.5194/acp-9-3825-2009, 2009.

Cooper, O., Forster, C., Parrish, D., Dunlea, E., Hübler, G., Fehsenfeld, F., Holloway, J., Oltmans, S.,
650   Johnson, B., Wimmers, A., and Horowitz, L.: On the life cycle of a stratospheric intrusion and its

dispersion into polluted warm conveyor belts, J. Geophys. Res.-Atmos., 109, https://doi.org/10.1029/2003JD004006, 2004.

Dennison, P. E., Brewer, S. C., Arnold, J. D., and Moritz, M. A.: Large wildfire trends in the western United States, 1984–2011, Geophys. Res. Lett., 41, 2928-2933, https://doi.org/10.1002/2014gl059576, 655   2014.

Dentener, F., Kinne, S., Bond, T., Boucher, O., Cofala, J., Generoso, S., Ginoux, P., Gong, S., Hoelzemann, J. J., Ito, A., Marelli, L., Penner, J. E., Putaud, J. P., Textor, C., Schulz, M., van der Werf, G. R., and Wilson, J.: Emissions of primary aerosol and precursor gases in the years 2000 and 1750 prescribed data-sets for AeroCom, Atmos. Chem. Phys., 6, 4321-4344, https://doi.org/10.5194/acp-6-4321-2006, 660   2006.

Donner, L. J., Wyman, B. L., Hemler, R. S., Horowitz, L. W., Ming, Y., Zhao, M., Golaz, J.-C., Ginoux, P., Lin, S.-J., Schwarzkopf, M. D., Austin, J., Alaka, G., Cooke, W. F., Delworth, T. L., Freidenreich, S. M., Gordon, C. T., Griffies, S. M., Held, I. M., Hurlin, W. J., Klein, S. A., Knutson, T. R., Langenhorst, A. R., Lee, H.-C., Lin, Y., Magi, B. I., Malyshev, S. L., Milly, P. C. D., Naik, V., Nath, 665   M. J., Pincus, R., Ploshay, J. J., Ramaswamy, V., Seman, C. J., Shevliakova, E., Sirutis, J. J., Stern, W. F., Stouffer, R. J., Wilson, R. J., Winton, M., Wittenberg, A. T., and Zeng, F.: The Dynamical Core, Physical Parameterizations, and Basic Simulation Characteristics of the Atmospheric Component AM3 of the GFDL Global Coupled Model CM3, J. Climate, 24, 3484-3519, https://doi.org/10.1175/2011jcli3955.1, 2011.

670   Eastham, S. D., Weisenstein, D. K., and Barrett, S. R. H.: Development and evaluation of the unified tropospheric–stratospheric chemistry extension (UCX) for the global chemistry-transport model GEOS-Chem, Atmos. Environ., 89, 52-63, https://doi.org/10.1016/j.atmosenv.2014.02.001, 2014.

Emery, C., Jung, J., Downey, N., Johnson, J., Jimenez, M., Yarwood, G., and Morris, R.: Regional and global modeling estimates of policy relevant background ozone over the United States, Atmos. 675   Environ., 47, 206-217, https://doi.org/10.1016/j.atmosenv.2011.11.012, 2012.

Fiore, A. M., Oberman, J. T., Lin, M. Y., Zhang, L., Clifton, O. E., Jacob, D. J., Naik, V., Horowitz, L. W., Pinto, J. P., and Milly, G. P.: Estimating North American background ozone in U.S. surface air with two independent global models: Variability, uncertainties, and recommendations, Atmos. Environ., 96, 284-300, https://doi.org/10.1016/j.atmosenv.2014.07.045, 2014.

680   Gong, X., Kaulfus, A., Nair, U., and Jaffe, D. A.: Quantifying O3 Impacts in Urban Areas Due to Wildfires Using a Generalized Additive Model, Environ. Sci. Technol., 51, 13216-13223, https://doi.org/10.1021/acs.est.7b03130, 2017.

Guenther, A., Karl, T., Harley, P., Wiedinmyer, C., Palmer, P. I., and Geron, C.: Estimates of global terrestrial isoprene emissions using MEGAN (Model of Emissions of Gases and Aerosols from 685   Nature), Atmos. Chem. Phys., 6, 3181-3210, https://doi.org/10.5194/acp-6-3181-2006, 2006.

Guo, J. J., Fiore, A. M., Murray, L. T., Jaffe, D. A., Schnell, J. L., Moore, C. T., and Milly, G. P.: Average versus high surface ozone levels over the continental USA: model bias, background influences, and interannual variability, Atmos. Chem. Phys., 18, 12123-12140, https://doi.org/10.5194/acp-18-12123-2018, 2018.

690   Herman, R. L., Webster, C. R., May, R. D., Scott, D. C., Hu, H., Moyer, E. J., Wennberg, P. O., Hanisco, T. F., Lanzendorf, E. J., Salawitch, R. J., Yung, Y. L., Margitan, J. J., and Bui, T. P.: Measurements of CO in the upper troposphere and lower stratosphere, Chemosphere - Global Change Science, 1, 173-183, https://doi.org/10.1016/S1465-9972(99)00008-2, 1999.

Hoesly, R. M., Smith, S. J., Feng, L., Klimont, Z., Janssens-Maenhout, G., Pitkanen, T., Seibert, J. J., Vu, 695   L., Andres, R. J., Bolt, R. M., Bond, T. C., Dawidowski, L., Kholod, N., Kurokawa, J. I., Li, M., Liu, L., Lu, Z., Moura, M. C. P., O'Rourke, P. R., and Zhang, Q.: Historical (1750–2014) anthropogenic

Atmospheric
Chemistry
and Physics
Discussions

emissions of reactive gases and aerosols from the Community Emissions Data System (CEDS), Geosci. Model Dev., 11, 369-408, https://doi.org/10.5194/gmd-11-369-2018, 2018.

700 Holzinger, R., Warneke, C., Hansel, A., Jordan, A., Lindinger, W., Scharffe, D. H., Schade, G., and Crutzen, P. J.: Biomass burning as a source of formaldehyde, acetaldehyde, methanol, acetone, acetonitrile, and hydrogen cyanide, Geophys. Res. Lett., 26, 1161-1164, https://doi.org/10.1029/1999gl900156, 1999.

Jacob, D. J., Logan, J. A., and Murti, P. P.: Effect of rising Asian emissions on surface ozone in the United States, Geophys. Res. Lett., 26, 2175-2178, https://doi.org/10.1029/1999GL900450, 1999.

705 Jaffe, D. A., Wigder, N., Downey, N., Pfister, G., Boynard, A., and Reid, S. B.: Impact of Wildfires on Ozone Exceptional Events in the Western U.S, Environ. Sci. Technol., 47, 11065-11072, https://doi.org/10.1021/es402164f, 2013.

Jaffe, D. A., Cooper, O. R., Fiore, A. M., Henderson, B. H., Tonneson, G. S., Russell, A. G., Henze, D. K., Langford, A. O., Lin, M., and Moore, T.: Scientific assessment of background ozone over the U.S.:
710 Implications for air quality management, Elementa: Science of the Anthropocene, 6(1), http://doi.org/10.1525/elementa.309, 2018.

Kleinman, L. I., Daum, P. H., Lee, Y.-N., Nunnermacker, L. J., Springston, S. R., Weinstein-Lloyd, J., and Rudolph, J.: Ozone production efficiency in an urban area, J. Geophys. Res.-Atmos., 107, ACH 23-21-ACH 23-12, https://doi.org/10.1029/2002jd002529, 2002.

715 Langford, A. O., Aikin, K. C., Eubank, C. S., and Williams, E. J.: Stratospheric contribution to high surface ozone in Colorado during springtime, Geophys. Res. Lett., 36, L12801, https://doi.org/10.1029/2009GL038367, 2009.

Langford, A. O., Senff, C. J., Alvarez, R. J., Banta, R. M., and Hardesty, R. M.: Long-range transport of ozone from the Los Angeles Basin: A case study, Geophys. Res. Lett., 37,
720 https://doi.org/10.1029/2010GL042507, 2010.

Langford, A. O., Brioude, J., Cooper, O. R., Senff, C. J., Alvarez, R. J., Hardesty, R. M., Johnson, B. J., and Oltmans, S. J.: Stratospheric influence on surface ozone in the Los Angeles area during late spring and early summer of 2010, J. Geophys. Res.-Atmos., 117, https://doi.org/10.1029/2011JD016766, 2012.

725 Langford, A. O., Senff, C. J., Alvarez, R. J., Brioude, J., Cooper, O. R., Holloway, J. S., Lin, M. Y., Marchbanks, R. D., Pierce, R. B., Sandberg, S. P., Weickmann, A. M., and Williams, E. J.: An overview of the 2013 Las Vegas Ozone Study (LVOS): Impact of stratospheric intrusions and long-range transport on surface air quality, Atmos. Environ., 109, 305-322, https://doi.org/10.1016/j.atmosenv.2014.08.040, 2015.

730 Langford, A. O., Alvarez II, R. J., Brioude, J., Fine, R., Gustin, M. S., Lin, M. Y., Marchbanks, R. D., Pierce, R. B., Sandberg, S. P., Senff, C. J., Weickmann, A. M., and Williams, E. J.: Entrainment of stratospheric air and Asian pollution by the convective boundary layer in the southwestern U.S, J. Geophys. Res.-Atmos., 122, 1312-1337, https://doi.org/10.1002/2016JD025987, 2017.

Langford, A. O., Alvarez II, R. J., Kirgis, G., Senff, C. J., Caputi, D., Conley, S. A., Faloona, I. C., Iraci,
735 L. T., Marrero, J. E., McNamara, M. E., Ryoo, J. M., and Yates, E. L.: Intercomparison of lidar, aircraft, and surface ozone measurements in the San Joaquin Valley during the California Baseline Ozone Transport Study (CABOTS), Atmos. Meas. Tech., 12, 1889-1904, https://doi.org/10.5194/amt-12-1889-2019, 2019.

Li, J., Mao, J., Min, K.-E., Washenfelder, R. A., Brown, S. S., Kaiser, J., Keutsch, F. N., Volkamer, R.,
740 Wolfe, G. M., Hanisco, T. F., Pollack, I. B., Ryerson, T. B., Graus, M., Gilman, J. B., Lerner, B. M., Warneke, C., de Gouw, J. A., Middlebrook, A. M., Liao, J., Welti, A., Henderson, B. H., McNeill, V. F., Hall, S. R., Ullmann, K., Donner, L. J., Paulot, F., and Horowitz, L. W.: Observational constraints

on glyoxal production from isoprene oxidation and its contribution to organic aerosol over the Southeast United States, J. Geophys. Res.-Atmos., 121, 9849-9861,
745   https://doi.org/10.1002/2016jd025331, 2016.

Li, M., Zhang, Q., Kurokawa, J. I., Woo, J. H., He, K., Lu, Z., Ohara, T., Song, Y., Streets, D. G., Carmichael, G. R., Cheng, Y., Hong, C., Huo, H., Jiang, X., Kang, S., Liu, F., Su, H., and Zheng, B.: MIX: a mosaic Asian anthropogenic emission inventory under the international collaboration framework of the MICS-Asia and HTAP, Atmos. Chem. Phys., 17, 935-963,
750   https://doi.org/10.5194/acp-17-935-2017, 2017.

Lin, M., Fiore, A. M., Cooper, O. R., Horowitz, L. W., Langford, A. O., Levy II, H., Johnson, B. J., Naik, V., Oltmans, S. J., and Senff, C. J.: Springtime high surface ozone events over the western United States: Quantifying the role of stratospheric intrusions, J. Geophys. Res.-Atmos., 117, D00V22, https://doi.org/10.1029/2012JD018151, 2012a.

755   Lin, M., Fiore, A. M., Horowitz, L. W., Cooper, O. R., Naik, V., Holloway, J., Johnson, B. J., Middlebrook, A. M., Oltmans, S. J., Pollack, I. B., Ryerson, T. B., Warner, J. X., Wiedinmyer, C., Wilson, J., and Wyman, B.: Transport of Asian ozone pollution into surface air over the western United States in spring, J. Geophys. Res.-Atmos., 117, D00V07, https://doi.org/10.1029/2011JD016961, 2012b.

Lin, M., Fiore, A. M., Horowitz, L. W., Langford, A. O., Oltmans, S. J., Tarasick, D., and Rieder, H. E.:
760   Climate variability modulates western US ozone air quality in spring via deep stratospheric intrusions, Nat. Commun., 6, 7105, https://doi.org/10.1038/ncomms8105, 2015a.

Lin, M., Horowitz, L. W., Cooper, O. R., Tarasick, D., Conley, S., Iraci, L. T., Johnson, B., Leblanc, T., Petropavlovskikh, I., and Yates, E. L.: Revisiting the evidence of increasing springtime ozone mixing ratios in the free troposphere over western North America, Geophys. Res. Lett., 42, 2015GL065311,
765   10.1002/2015GL065311, 2015b.

Lin, M., Horowitz, L. W., Payton, R., Fiore, A. M., and Tonnesen, G.: US surface ozone trends and extremes from 1980 to 2014: quantifying the roles of rising Asian emissions, domestic controls, wildfires, and climate, Atmos. Chem. Phys., 17, 2943-2970, https://doi.org/10.5194/acp-17-2943-2017, 2017.

770   Lin, M., Malyshev, S., Shevliakova, E., Paulot, F., Horowitz, L. W., Fares, S., Mikkelsen, T. N., and Zhang, L.: Sensitivity of ozone dry deposition to ecosystem-atmosphere interactions: A critical appraisal of observations and simulations, Global Biogeochem. Cy., 30, https://doi.org/10.1029/2018gb006157, 2019.

Liu, F., Zhang, Q., van der A, R. J., Zheng, B., Tong, D., Yan, L., Zheng, Y., and He, K.: Recent reduction
775   in NO x emissions over China: synthesis of satellite observations and emission inventories, Environ. Res. Lett., 11, 114002, https://doi.org/10.1088/1748-9326/11/11/114002, 2016.

Mao, J., Horowitz, L. W., Naik, V., Fan, S., Liu, J., and Fiore, A. M.: Sensitivity of tropospheric oxidants to biomass burning emissions: implications for radiative forcing, Geophys. Res. Lett., 40, 1241-1246, https://doi.org/10.1002/grl.50210, 2013a.

780   Mao, J., Paulot, F., Jacob, D. J., Cohen, R. C., Crounse, J. D., Wennberg, P. O., Keller, C. A., Hudman, R. C., Barkley, M. P., and Horowitz, L. W.: Ozone and organic nitrates over the eastern United States: Sensitivity to isoprene chemistry, J. Geophys. Res.-Atmos., 118, 11,256-211,268, https://doi.org/10.1002/jgrd.50817, 2013b.

McLinden, C. A., Olsen, S. C., Hannegan, B., Wild, O., Prather, M. J., and Sundet, J.: Stratospheric ozone
785   in 3-D models: A simple chemistry and the cross-tropopause flux, J. Geophys. Res.-Atmos., 105, 14653-14665, https://doi.org/10.1029/2000jd900124, 2000.

Morgenstern, O., Zeng, G., Luke Abraham, N., Telford, P. J., Braesicke, P., Pyle, J. A., Hardiman, S. C., O'Connor, F. M., and Johnson, C. E.: Impacts of climate change, ozone recovery, and increasing

methane on surface ozone and the tropospheric oxidizing capacity, J. Geophys. Res.-Atmos., 118, 1028-1041, https://doi.org/10.1029/2012jd018382, 2013.

Murray, L. T., Jacob, D. J., Logan, J. A., Hudman, R. C., and Koshak, W. J.: Optimized regional and interannual variability of lightning in a global chemical transport model constrained by LIS/OTD satellite data, J. Geophys. Res.-Atmos., 117, https://doi.org/10.1029/2012jd017934, 2012.

Naik, V., Horowitz, L. W., Fiore, A. M., Ginoux, P., Mao, J., Aghedo, A. M., and Levy II, H.: Impact of preindustrial to present-day changes in short-lived pollutant emissions on atmospheric composition and climate forcing, J. Geophys. Res.-Atmos., 118, 8086-8110, https://doi.org/10.1002/jgrd.50608, 2013.

Parrish, D. D., Trainer, M., Holloway, J. S., Yee, J. E., Warshawsky, M. S., Fehsenfeld, F. C., Forbes, G. L., and Moody, J. L.: Relationships between ozone and carbon monoxide at surface sites in the North Atlantic region, J. Geophys. Res.-Atmos., 103, 13357-13376, https://doi.org/10.1029/98JD00376, 1998.

Paulot, F., Ginoux, P., Cooke, W. F., Donner, L. J., Fan, S., Lin, M. Y., Mao, J., Naik, V., and Horowitz, L. W.: Sensitivity of nitrate aerosols to ammonia emissions and to nitrate chemistry: implications for present and future nitrate optical depth, Atmos. Chem. Phys., 16, 1459-1477, https://doi.org/10.5194/acp-16-1459-2016, 2016.

Paulot, F., Paynter, D., Ginoux, P., Naik, V., Whitburn, S., Van Damme, M., Clarisse, L., Coheur, P.-F., and Horowitz, L. W.: Gas-aerosol partitioning of ammonia in biomass burning plumes: Implications for the interpretation of spaceborne observations of ammonia and the radiative forcing of ammonium nitrate, Geophys. Res. Lett., 44, 8084-8093, https://doi.org/10.1002/2017GL074215, 2017.

Prather, M. J., Zhu, X., Tang, Q., Hsu, J., and Neu, J. L.: An atmospheric chemist in search of the tropopause, J. Geophys. Res.-Atmos., 116, https://doi.org/10.1029/2010JD014939, 2011.

Schnell, J. L., Naik, V., Horowitz, L. W., Paulot, F., Mao, J., Ginoux, P., Zhao, M., and Ram, K.: Exploring the relationship between surface PM2.5 and meteorology in Northern India, Atmos. Chem. Phys., 18, 10157-10175, https://doi.org/10.5194/acp-18-10157-2018, 2018.

Singh, H. B., Cai, C., Kaduwela, A., Weinheimer, A., and Wisthaler, A.: Interactions of fire emissions and urban pollution over California: Ozone formation and air quality simulations, Atmos. Environ., 56, 45-51, https://doi.org/10.1016/j.atmosenv.2012.03.046, 2012.

Travis, K. R., Jacob, D. J., Fisher, J. A., Kim, P. S., Marais, E. A., Zhu, L., Yu, K., Miller, C. C., Yantosca, R. M., Sulprizio, M. P., Thompson, A. M., Wennberg, P. O., Crounse, J. D., St. Clair, J. M., Cohen, R. C., Laughner, J. L., Dibb, J. E., Hall, S. R., Ullmann, K., Wolfe, G. M., Pollack, I. B., Peischl, J., Neuman, J. A., and Zhou, X.: Why do models overestimate surface ozone in the Southeast United States?, Atmos. Chem. Phys., 16, 13561-13577, https://doi.org/10.5194/acp-16-13561-2016, 2016.

Trickl, T., Vogelmann, H., Fix, A., Schäfler, A., Wirth, M., Calpini, B., Levrat, G., Romanens, G., Apituley, A., Wilson, K. M., Begbie, R., Reichardt, J., Vömel, H., and Sprenger, M.: How stratospheric are deep stratospheric intrusions? LUAMI 2008, Atmos. Chem. Phys., 16, 8791-8815, https://doi.org/10.5194/acp-16-8791-2016, 2016.

U.S. Environmental Protection Agency: Treatment of data influenced by exceptional events, edited by U. S. Environmental Protection Agency, Research Triangle Park, North Carolina, United States of America, 68216-68282 pp., 2016.

Wang, Y. X., McElroy, M. B., Jacob, D. J., and Yantosca, R. M.: A nested grid formulation for chemical transport over Asia: Applications to CO, J. Geophys. Res.-Atmos., 109, https://doi.org/10.1029/2004JD005237, 2004.

West, J. J., Fiore, A. M., Horowitz, L. W., and Mauzerall, D. L.: Global health benefits of mitigating ozone pollution with methane emission controls, P. Natl. Acad. Sci. USA, 103, 3988-3993, https://doi.org/10.1073/pnas.0600201103, 2006.

Westerling, A. L., Hidalgo, H. G., Cayan, D. R., and Swetnam, T. W.: Warming and Earlier Spring Increase Western U.S. Forest Wildfire Activity, Science, 313, 940-943, https://doi.org/10.1126/science.1128834, 2006.

Wiedinmyer, C., Akagi, S. K., Yokelson, R. J., Emmons, L. K., Al-Saadi, J. A., Orlando, J. J., and Soja, A. J.: The Fire INventory from NCAR (FINN): a high resolution global model to estimate the emissions from open burning, Geosci. Model Dev., 4, 625-641, https://doi.org/10.5194/gmd-4-625-2011, 2011.

Wild, R. J., Dubé, W. P., Aikin, K. C., Eilerman, S. J., Neuman, J. A., Peischl, J., Ryerson, T. B., and Brown, S. S.: On-road measurements of vehicle NO2/NOx emission ratios in Denver, Colorado, USA, Atmos. Environ., 148, 182-189, https://doi.org/10.1016/j.atmosenv.2016.10.039, 2017.

Zhang, L., Jacob, D. J., Boersma, K. F., Jaffe, D. A., Olson, J. R., Bowman, K. W., Worden, J. R., Thompson, A. M., Avery, M. A., Cohen, R. C., Dibb, J. E., Flock, F. M., Fuelberg, H. E., Huey, L. G., McMillan, W. W., Singh, H. B., and Weinheimer, A. J.: Transpacific transport of ozone pollution and the effect of recent Asian emission increases on air quality in North America: an integrated analysis using satellite, aircraft, ozonesonde, and surface observations, Atmos. Chem. Phys., 8, 6117-6136, https://doi.org/10.5194/acp-8-6117-2008, 2008.

Zhang, L., Jacob, D. J., Downey, N. V., Wood, D. A., Blewitt, D., Carouge, C. C., van Donkelaar, A., Jones, D. B. A., Murray, L. T., and Wang, Y.: Improved estimate of the policy-relevant background ozone in the United States using the GEOS-Chem global model with $1/2° \times 2/3°$ horizontal resolution over North America, Atmos. Environ., 45, 6769-6776, https://doi.org/10.1016/j.atmosenv.2011.07.054, 2011.

Zhang, L., Jacob, D. J., Yue, X., Downey, N. V., Wood, D. A., and Blewitt, D.: Sources contributing to background surface ozone in the US Intermountain West, Atmos. Chem. Phys., 14, 5295-5309, https://doi.org/10.5194/acp-14-5295-2014, 2014.

Zhao, M., Golaz, J.-C., Held, I. M., Ramaswamy, V., Lin, S.-J., Ming, Y., Ginoux, P., Wyman, B., Donner, L. J., Paynter, D., and Guo, H.: Uncertainty in Model Climate Sensitivity Traced to Representations of Cumulus Precipitation Microphysics, J. Climate, 29, 543-560, https://doi.org/10.1175/jcli-d-15-0191.1, 2016.

Zhao, M., Golaz, J.-C., Held, I. M., Guo, H., Balaji, V., Benson, R., Chen, J.-H., Chen, X., Donner, L. J., Dunne, J. P., Dunne, K., Durachta, J., Fan, S.-M., Freidenreich, S. M., Garner, S. T., Ginoux, P., Harris, L. M., Horowitz, L. W., Krasting, J. P., Langenhorst, A. R., Liang, Z., Lin, P., Lin, S.-J., Malyshev, S. L., Mason, E., Milly, P. C. D., Ming, Y., Naik, V., Paulot, F., Paynter, D., Phillipps, P., Radhakrishnan, A., Ramaswamy, V., Robinson, T., Schwarzkopf, D., Seman, C. J., Shevliakova, E., Shen, Z., Shin, H., Silvers, L. G., Wilson, J. R., Winton, M., Wittenberg, A. T., Wyman, B., and Xiang, B.: The GFDL Global Atmosphere and Land Model AM4.0/LM4.0: 1. Simulation Characteristics With Prescribed SSTs, Journal of Advances in Modeling Earth Systems, 10, 691-734, https://doi.org/10.1002/2017ms001208, 2018a.

Zhao, M., Golaz, J.-C., Held, I. M., Guo, H., Balaji, V., Benson, R., Chen, J.-H., Chen, X., Donner, L. J., Dunne, J. P., Dunne, K., Durachta, J., Fan, S.-M., Freidenreich, S. M., Garner, S. T., Ginoux, P., Harris, L. M., Horowitz, L. W., Krasting, J. P., Langenhorst, A. R., Liang, Z., Lin, P., Lin, S.-J., Malyshev, S. L., Mason, E., Milly, P. C. D., Ming, Y., Naik, V., Paulot, F., Paynter, D., Phillipps, P., Radhakrishnan, A., Ramaswamy, V., Robinson, T., Schwarzkopf, D., Seman, C. J., Shevliakova, E., Shen, Z., Shin, H., Silvers, L. G., Wilson, J. R., Winton, M., Wittenberg, A. T., Wyman, B., and Xiang, B.: The GFDL

880   Global Atmosphere and Land Model AM4.0/LM4.0: 2. Model Description, Sensitivity Studies, and
   Tuning Strategies, Journal of Advances in Modeling Earth Systems, 10, 735-769,
       https://doi.org/10.1002/2017ms001209, 2018b.

Table 1. List of high-O$_3$ events above 65 ppbv in the greater Las Vegas region during April-June 2017 (unit: ppbv).

| Events	MDA8 O$_3$ (1-min max) at Angel Peak	Simulated MDA8 O$_3$ (USB) at Angel Peak: AM4 vs. GC	MDA8 O$_3$ at Clark County sites	Maximum MDA8 O$_3$ at rural sites in affected regions	Observed ΔO$_3$/ΔCO	Sonde; Lidar	Surface impacts
Stratospheric intrusions							
April 22-23	-	66 vs. 53 (60 vs. 47)	SM Youth Camp: 70; Green Valley: 67	**Apr 22: WY:** Centennial (76); **CO:** Mesa Verde NP (72), Gothic (82) **Apr 23: WY:** Centennial (75); **CO:** Rocky Mt. NP (70); **CA:** Joshua Tree (76)	-	-	Fig. S6
May 13-14	-	66 vs. 52 (62 vs. 48)	May 13: SM Youth Camp: 70; May 14: SM Youth Camp: 71	**May 13: CA:** Joshua Tree (74); **UT:** AQS site: Zion NP (69) **May 14: NV:** Great Basin NP (65)	-	-	Fig. S6
June 11-13	June 11: 66 (84);	65 vs. 47 (58 vs. 42)	Jun 11: SM Youth Camp: 64	**Jun 12: WY:** Centennial (70); **CO:** Mesa Verde (69) **Jun 13**: **WY:** Centennial (65); **AZ:** Petrified Forest (65); AQS sites: Payson (76); **NM:** AQS sites: Cayote (71)	-3.79 (Fig. 5a)	Figs. 6-7a	Fig. 8
June 14	73 (80)	69 vs. 57 (53 vs. 50)	Joe Neal: 74 North LV Airport: 73, Walter Johnson: 71	**CA:** Joshua Tree (95); **AZ:** Petrified Forest (71); **NM:** site: Bernalillo (71)	0.75 (Fig. 5b)	Fig. 7b	Fig. 8
Wildfires							
June 22	67 (83)	58 vs. 76 (44 vs. 62)	Joe Neal: 78 North LV Airport: 82	**CA:** Sequoia NP (86); Joshua Tree (74)	0.015 (Fig. 5e)	Fig. 9a	Fig. 10a
Regional/local pollution events							
June 2	71 (78)	61 vs. 64 (51 vs. 49)	Joe Neal: 66 Walter Johnson: 69	**CA:** Joshua Tree (68, Jun 1: 79)	1.09 (Fig. S4)	Fig. S10	Fig. S11
June 16	72 (82)	65 vs. 63 (46 vs. 54)	Joe Neal: 75 Palo Verde: 75	**CA:** Joshua Tree (98); **AZ:** Petrified Forest (65), AQS site: Payson (76)	0.68-0.70 (Figs. 5c-d)	Fig. 9b	Fig. 10b
June 29-30	June 29: 71 (78) June 30: 75 (86)	55 vs. 62 (41 vs. 54)	Jun 29: Joe Neal: 70; North LV Airport: 74 Jun 30: Joe Neal: 75; Walter Johnson: 75	**Jun 29**: **CA:** Sequoia NP (74); Joshua Tree (75) **Jun 30**: **CA:** Sequoia NP (83); Joshua Tree (96); **AZ:** Grand Canyon (66)	0.69-1.07 (Fig. S4)	Fig. S10	Fig. S11
Long-range transport of Asian pollution							

29

Atmospheric
Chemistry
and Physics
Discussions

May 24	65 (74)	62 vs. 68 (48 vs. 54)	Arden Peak: 72, SM Youth Camp: 66, Jean: 66, Palo Verde: 65	**CA:** Yosemite NP (70); **ID:** AQS site: Butte (69); **WY:** Yellowstone NP (64); **UT:** AQS site: Zion NP (65)	-	Fig. 12a	Fig. 13a
Unattributed event							
June 28	68 (84)	53 vs. 59 (43 vs. 54)	Joe Neal: 75; North LV Airport: 74	**CA:** Sequoia NP (70); **AZ:** Grand Canyon (66)	1.92 (Fig. 5f)	Fig. 12b	Fig. 13b
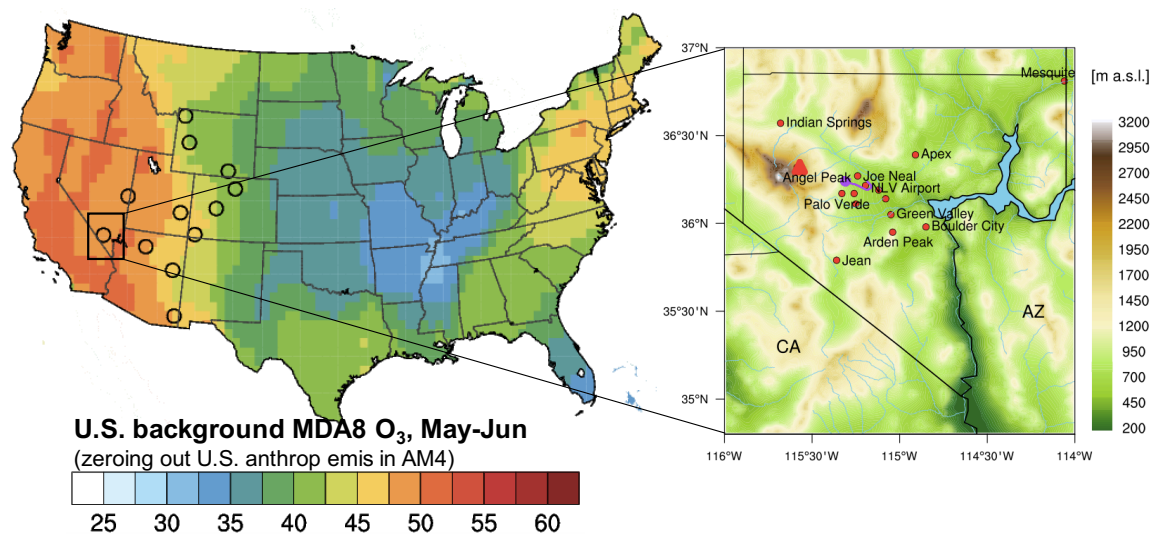
Figure 1. (Left) Mean U.S. background MDA8 O_3 (ppbv) during FAST-LVOS (May−June, 2017) estimated by zeroing out U.S. anthropogenic emissions in the global high-resolution (~50 km × 50 km) version of the GFDL-AM4 model (circles denote 12 selected high-elevation CASTNet sites); (Right) Topographic map of Clark County displaying the locations of Angel Peak (filled triangle) and regulatory O_3 monitoring sites (filled circles). The purple trace denotes the Scientific Aviation flight track during 19:15-19:35 UTC of June 28, 2017. The topographic data is from NOAA's National Centers for Environmental Information (http://www.ngdc.noaa.gov/mgg/global).
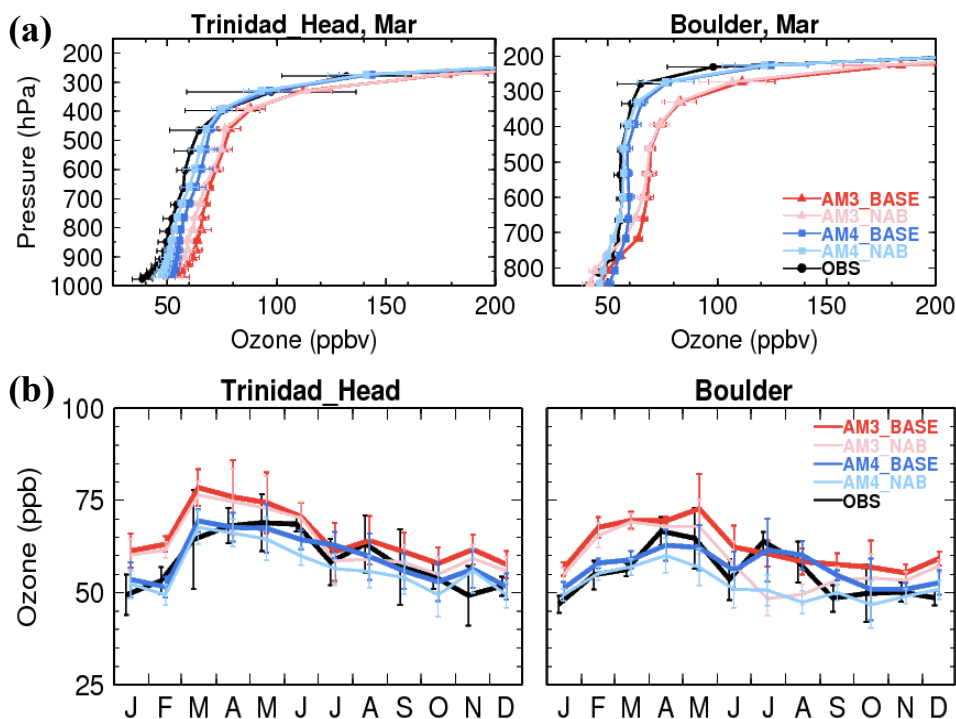
Figure 2. (a) Vertical profiles of O₃ in March and (b) monthly mean O₃ in the middle troposphere (500–430 hPa) at Trinidad Head, California and Boulder, Colorado during 2010–2014 as observed (black) and simulated by GFDL-AM3 (red; AM3_BASE; Lin et al., 2017) and GFDL-AM4 (blue; AM4_BASE), together with simulated North American Background O₃ (NAB; estimated with North American anthropogenic emissions zeroed out). The bars represent the standard deviations of monthly values during 2010–2014.
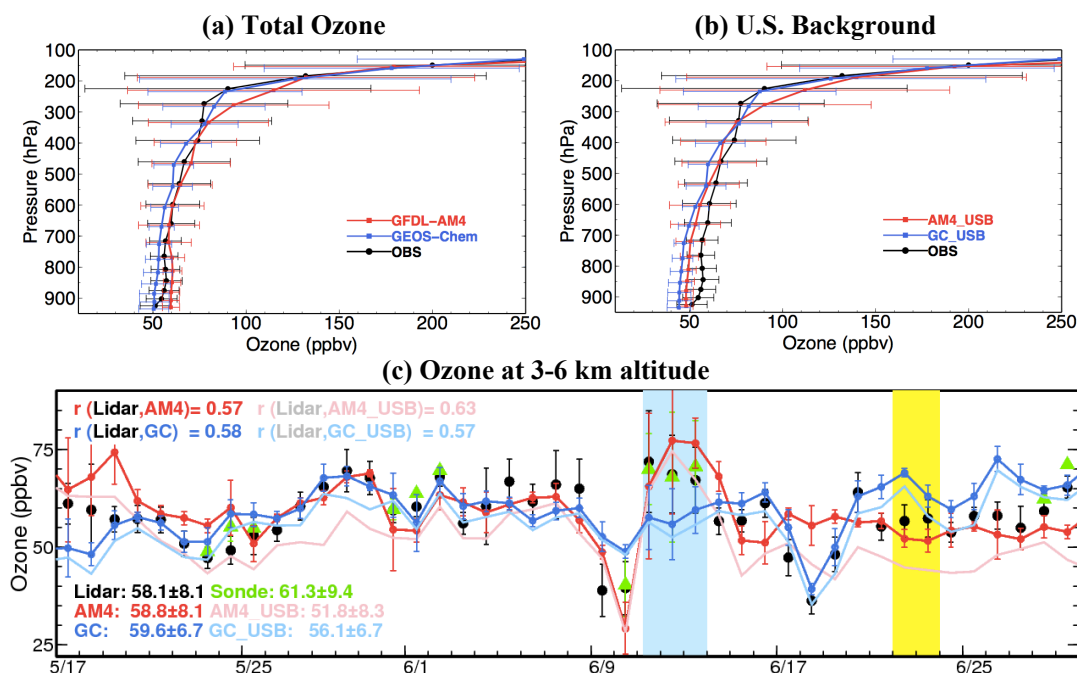
Figure 3. (a) Mean vertical O$_3$ profiles at Joe Neal as observed with ozonesondes (black; 30 launches) and simulated with GFDL-AM4 (red) and GEOS-Chem (blue) during FAST-LVOS (May–June 2017). Horizontal bars represent the standard deviations across daily profiles; (b) Same as (a), but showing U.S. background (USB) O$_3$ estimated by the two models. (c) Time series of O$_3$ averaged over 3-6 km altitude above NLVA during FAST-LVOS as observed (black: lidar; green: ozonesonde) and simulated with GFDL-AM4 (thick red line) and GEOS-Chem (thick dark blue line), together with simulated USB O$_3$ (light lines). Here and in other figures, AM4_USB represents USB estimated by GFDL-AM4 and GC_USB represents USB estimated by GEOS-Chem. The blue shading highlights the period with stratospheric intrusions and the yellow shading, the wildfire event. Vertical bars represent the standard deviations across hourly averages.
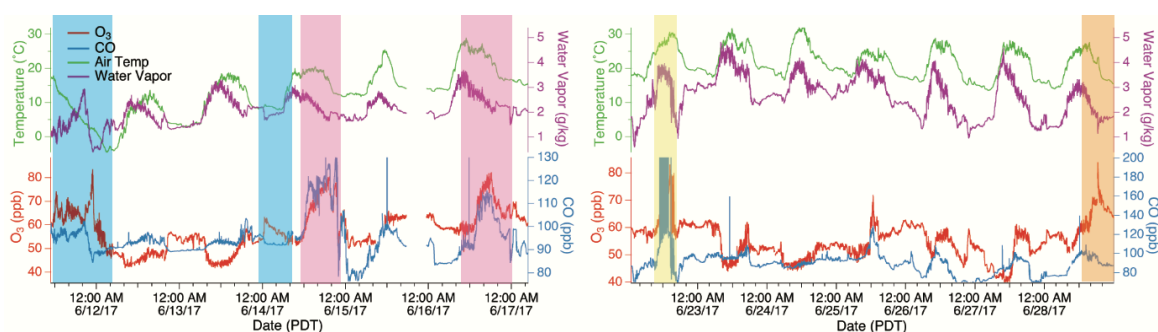
Figure 4. Time series of 1-minute averaged air temperature, water vapor, O_3, and CO mixing ratios measured by the NOAA mobile lab deployed at Angel Peak during June 11−16 and June 22−28, 2017, highlighting the periods with stratospheric influence (blue), regional anthropogenic pollution plumes (pink), wildfire plumes (yellow), and the unattributed pollution plume (orange). Data are shown in Pacific Daylight Time (PDT).

Atmospheric
Chemistry
and Physics
Discussions
Open Access
EGU
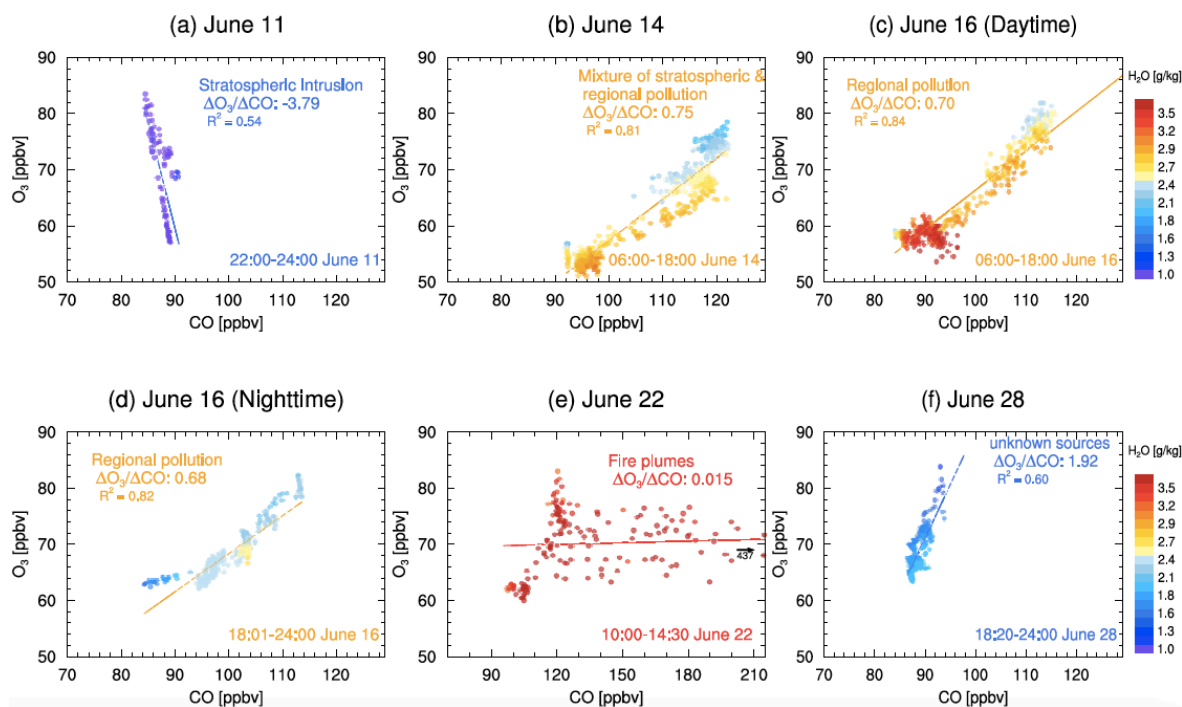
Figure 5. Scatter plots of 1-min average O_3 against CO measured at Angel Peak, color-coded by specific humidity, for air masses influenced by (a) STT on June 11; (b) regional pollution on June 14; (c) regional pollution plume during daytime (06:00–18:00) on June 16; (d) regional pollution during nighttime (18:01–24:00) on June 16; (e) wildfires on June 22; and (f) unattributed pollution on June 28.
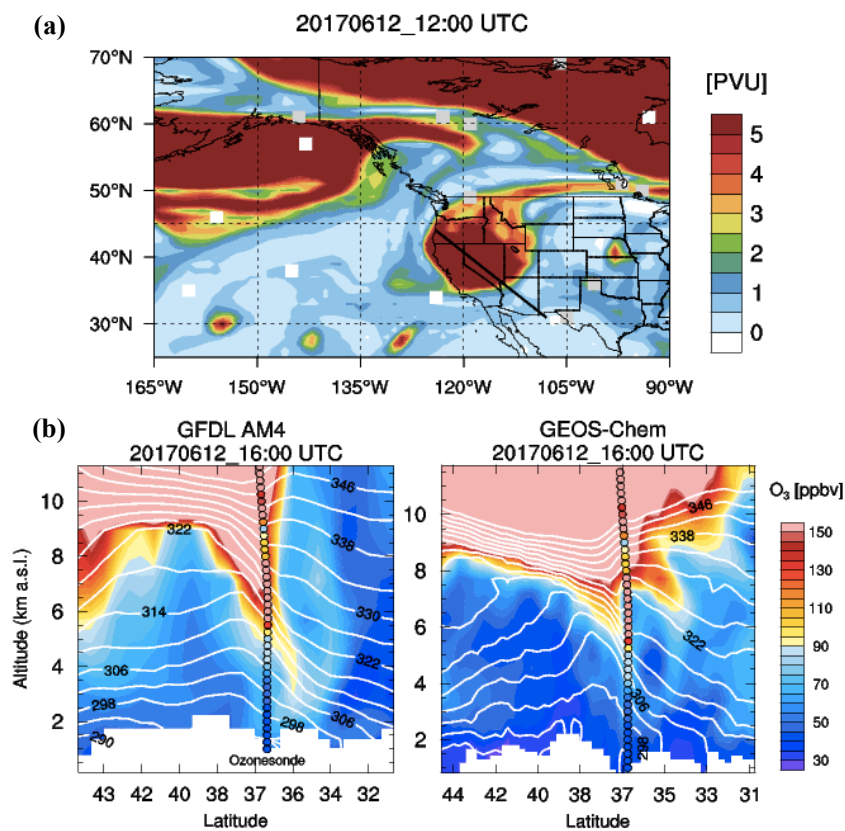
Figure 6. (a) Potential vorticity at 250 hPa on June 12 calculated from the NCEP-FNL reanalysis; (b) vertical distributions of O₃ (color shading) and isentropic surfaces (white lines) along a transect crossing Nevada (black line on PV map) simulated with GFDL-AM4 (left) and GEOS-Chem (right) on June 12. The color-coded circles denote ozonesonde observations at Joe Neal.

Atmospheric
Chemistry
and Physics
Discussions

(a) June 11-13 (STT)

(b) June 14 (STT and regional pollution)
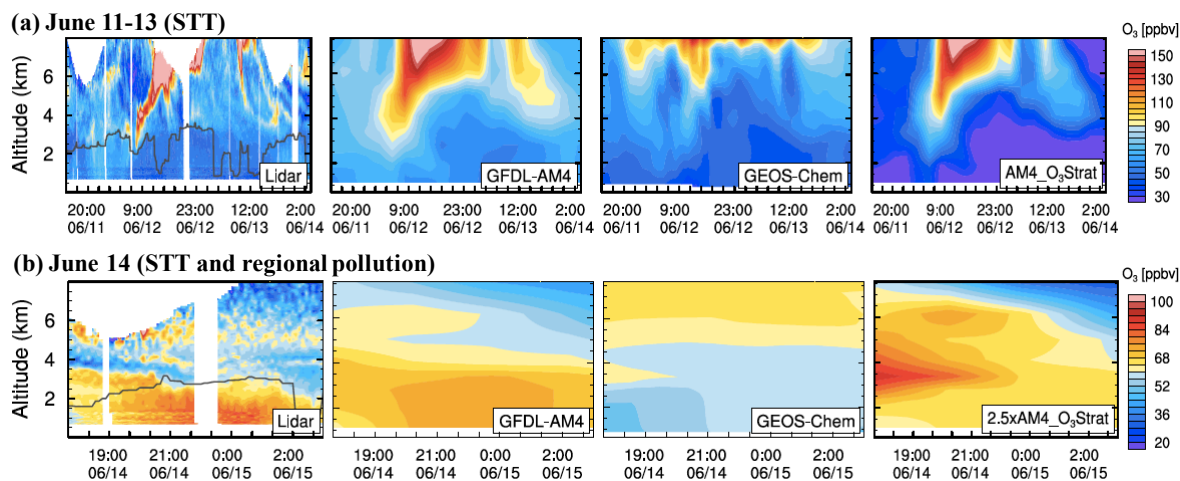
Figure 7. Time-height curtain plots of O_3 above NLVA as observed with TOPAZ lidar and simulated with GFDL-AM4 (~50 km × 50 km; interpolated from 3-hourly data) and GEOS-Chem (0.25° × 0.3125°; interpolated from hourly data) during the STT event on (a) June 11−13 and (b) June 14, 2017 (UTC). The rightmost panel shows AM4 stratospheric O_3 tracer (AM4_O_3Strat). Note that AM4_O_3Strat for June 14 is scaled by a factor of 2.5 for clarity. Here and in other figures, the solid black lines in the O_3 lidar plots represent boundary layer height inferred from the micro-Doppler lidar measurements.
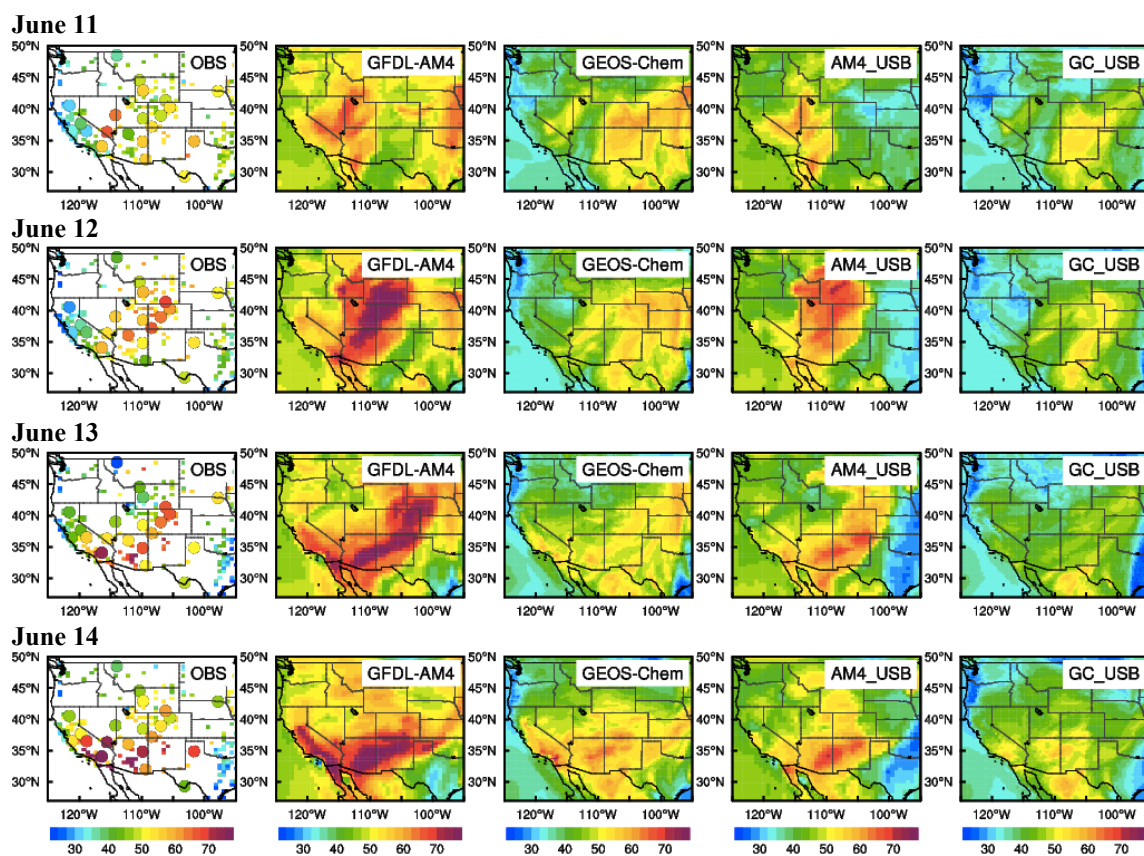
Figure 8. Maps of total MDA8 O$_3$ (ppbv) as observed and simulated with GFDL-AM4 and GEOS-Chem, along with the model-estimated USB level, during the STT event on June 11−14, 2017.

(a) June 22 (wildfires)

**(b) June 16 (regional anthropogenic pollution)**
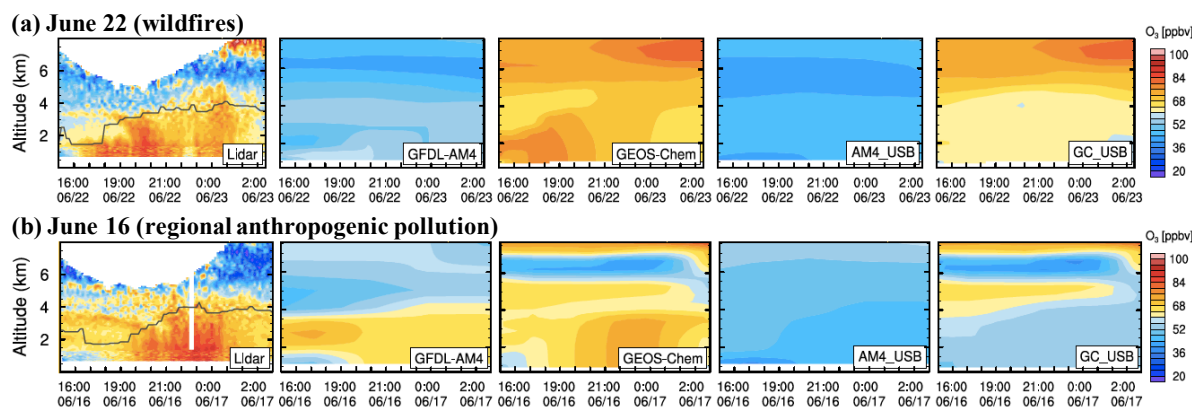
Figure 9. Same as Figure 7, but for (a) the wildfire event on June 22 and (b) the regional anthropogenic pollution event on June 16, 2017 (UTC). The right panels compare USB O_3 from the two models.

(a) June 22 (wildfires)

(b) June 16 (regional anthropogenic pollution)
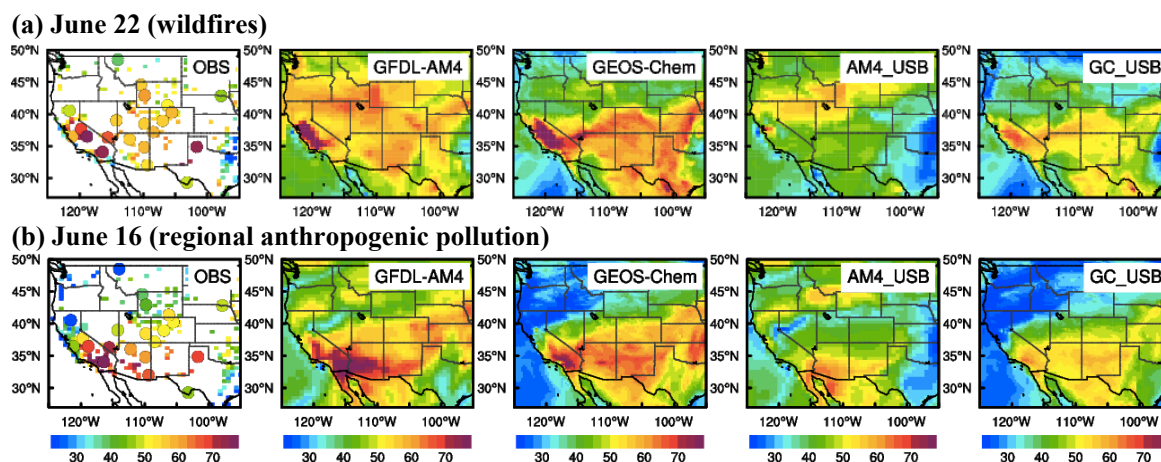
Figure 10. Same as Figure 8, but for (a) the wildfire event on June 22 and (b) the regional anthropogenic pollution event on June 16, 2017.

**(a) May 20-24**   **(b) June 23-27**
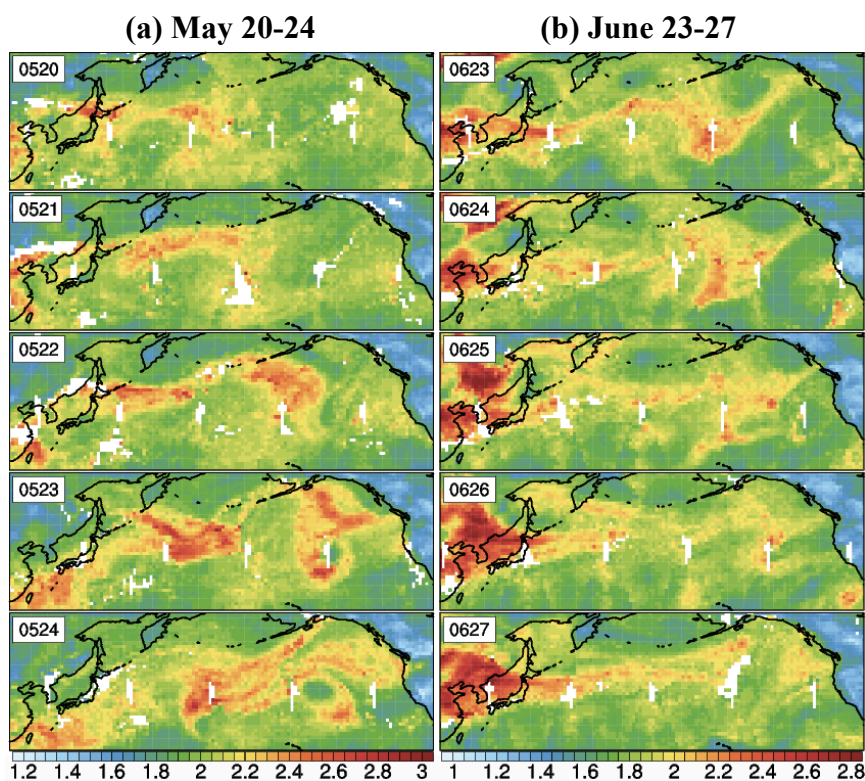
Figure 11. Trans-Pacific transport of Asian pollution plumes during (a) May 20–24 and (b) June 23–27, 2017, as seen in the NASA AIRS retrievals of CO total column (10^{18} molecules/cm^2; level 3 daily 1°×1° gridded products).

(a) May 24 (Asian pollution)


(b) June 28 (unattributed event)
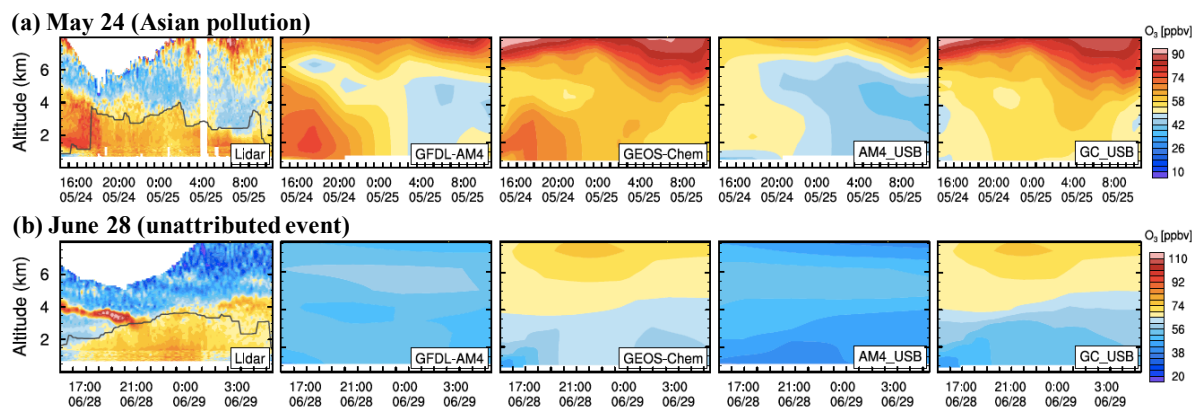
Figure 12. Same as Figure 7, but for (a) the Asian pollution event on May 24 and (b) the unattributed pollution event on June 28, 2017 (UTC).

(a) May 24 (Asian pollution)

**(b) June 28 (unattributed event)**
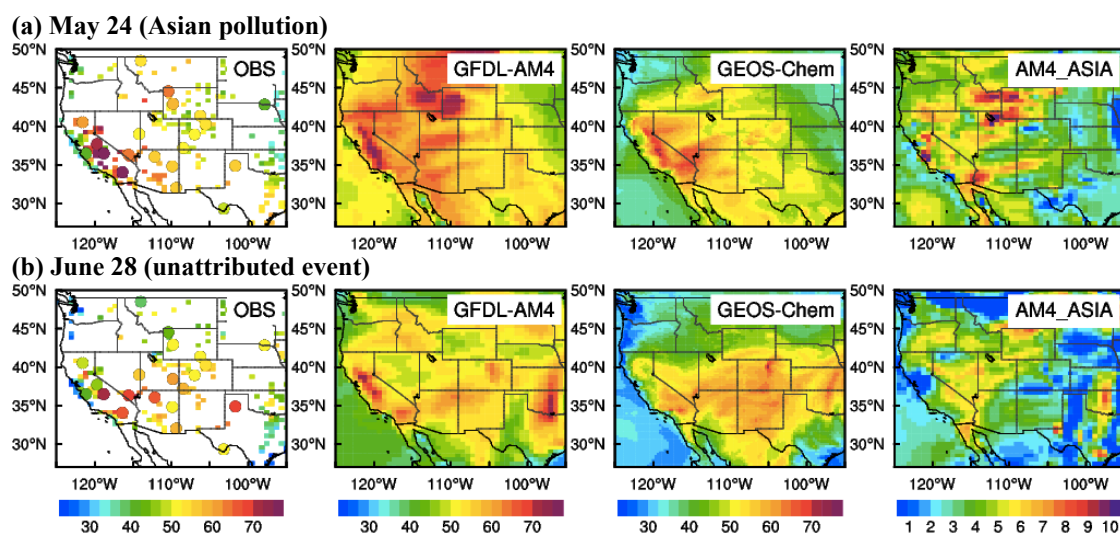
Figure 13. Same as Figure 8, but for (a) the Asian pollution event on May 24 and (b) the unattributed pollution event on June 28, 2017. The right panels show O_3 enhancements from Asian pollution estimated by GFDL-AM4.

43
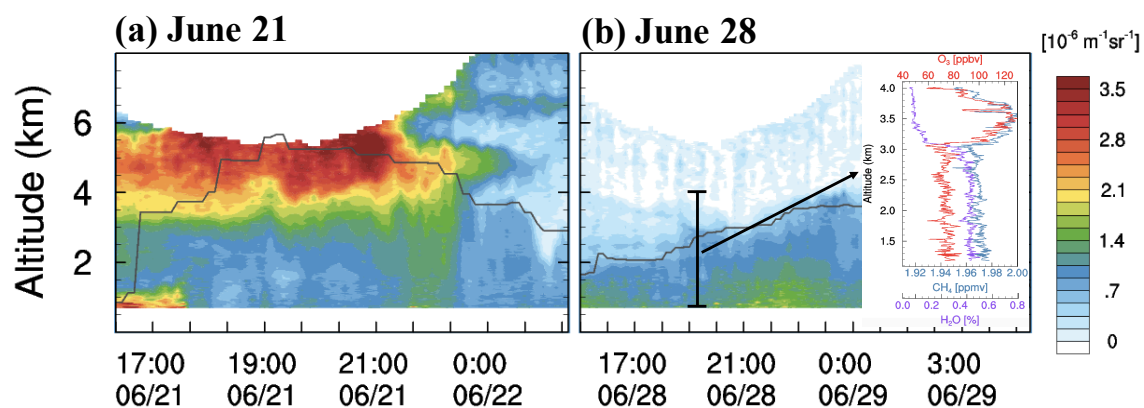
Figure 14. Time-height curtain plots of the particulate backscatter coefficients measured by TOPAZ during (a) the fire event on June 21−22 and (b) the unattributed event on June 28, 2017 at North Las Vegas Airport, together with water vapor (purple), CH_4 (blue), and O_3 (red) measured by the Scientific Aviation flight above the Las Vegas Valley during 19:15−19:35 June 28 (UTC) (flight track in Figure 1).
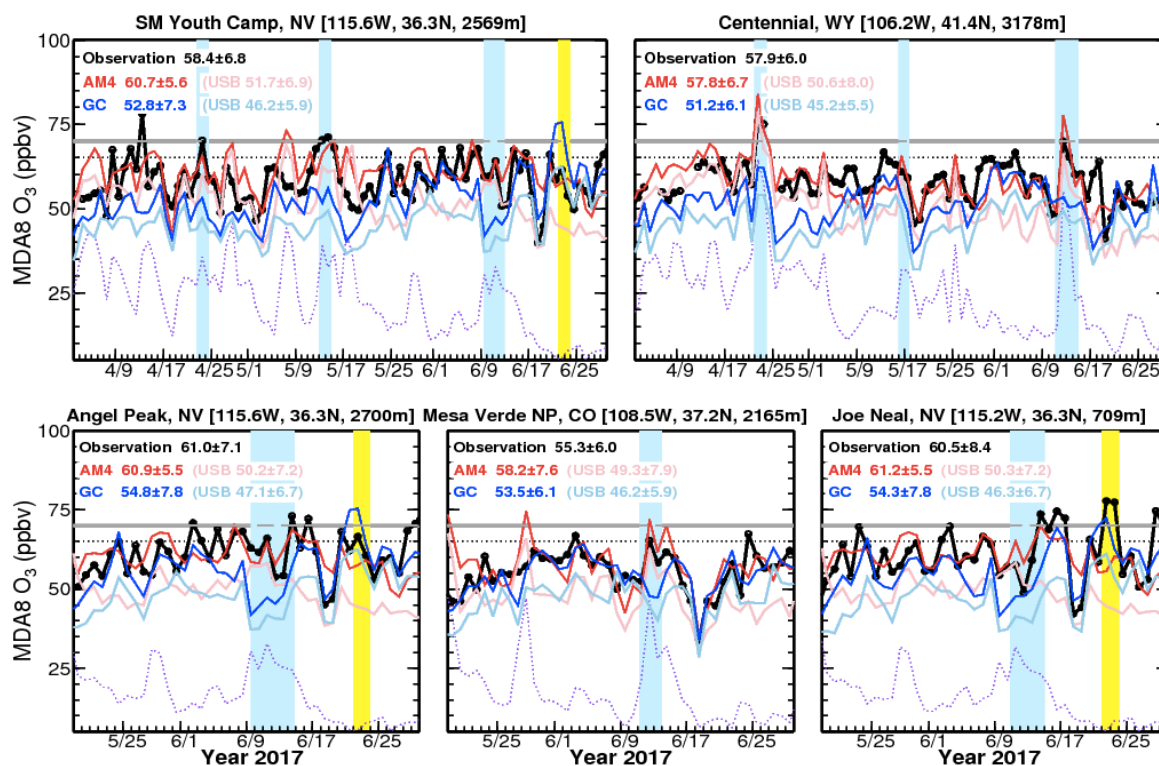
Figure 15. Time series of daily MDA8 O_3 at Spring Mountain Youth Camp and Centennial from April to June and at Angel Peak, Mesa Verde, and Joe Neal during the FAST-LVOS study period as observed (black) and simulated by GFDL-AM4 (red) and GEOS-Chem (blue), highlighting stratospheric intrusion events (blue shading) and wildfire events (yellow shading), together with USB O_3 estimated with the two models and stratospheric O_3 tracers estimated with GFDL-AM4 (dashed purple). The thick gray line denotes the current 70-ppbv NAAQS level and the dotted gray line a possible future standard of 65 ppbv.
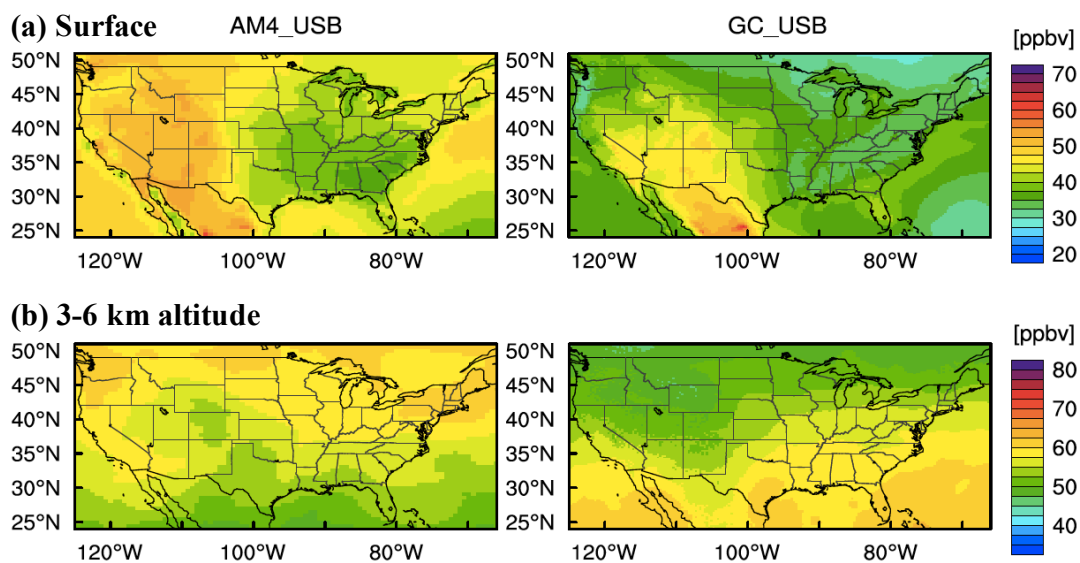
Figure 16. Spatial distributions of USB O_3 simulated with GFDL-AM4 and GEOS-Chem (a) at the surface and (b) at 3−6 km altitude during April−June, 2017.
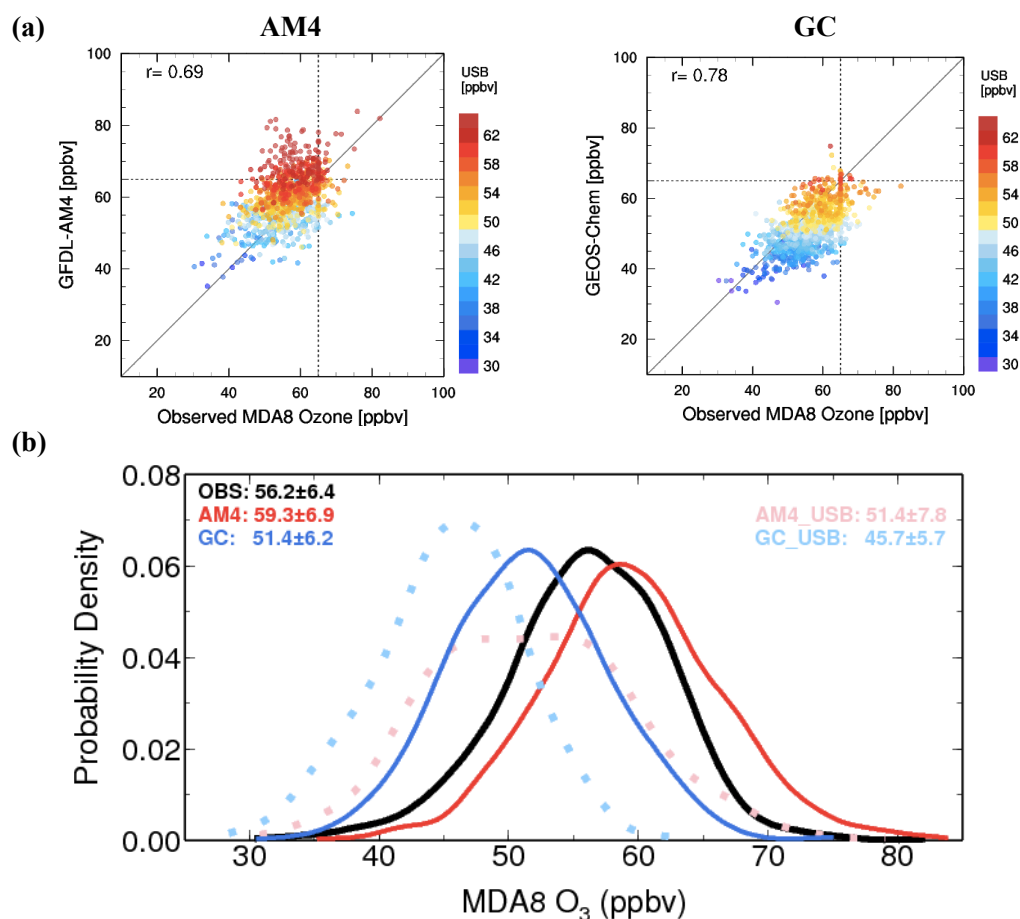
Figure 17. (a) Scatter plots of observed versus simulated daily MDA8 O$_3$, color-coded by USB O$_3$, at 12 WUS high-elevation sites (circles in Figure 1a) during April–June, 2017. The dashed lines mark the 65-ppbv threshold; (b) Probability density of daily MDA8 O$_3$ as observed (solid black) and simulated with GFDL-AM4 (solid red) and GEOS-Chem (solid blue), along with the distribution of USB O$_3$ estimated from each model (dotted lines).